

Saturable Purcell filter for circuit QED

Ivan Iakoupov* and Kazuki Koshino

*College of Liberal Arts and Sciences, Tokyo Medical and Dental University,
2-8-30 Konodai, Ichikawa, Chiba 272-0827, Japan*

(Dated: February 22, 2022)

We consider a typical circuit QED setup where a data artificial atom encodes a qubit and is dispersively coupled to a measurement resonator that in turn is coupled to a transmission line. We show theoretically that by placing a filter artificial atom in this transmission line, the effective decay of the data artificial atom into the transmission line (the Purcell decay) is suppressed. When strong control fields are present in the transmission line, the filter artificial atom is saturated and hence effectively switched off. This permits both control and measurement of the data artificial atom using a single transmission line, while maintaining the Purcell filtering capability and therefore a long coherence time of the data artificial atom in the absence of the control pulses. We also apply open systems optimal control techniques to optimize the π -pulse on the data artificial atom, achieving high fidelity. The considered setup is compatible with the frequency multiplexing, potentially enabling both control and measurement of several qubits using a single Purcell-filtered transmission line. Our work helps with the scalability of the superconducting quantum computers by decreasing the ratio between the number of qubits and the number of the required transmission lines. For the setups that already use one transmission line both for measurement and control, our work provides a way to filter out the qubit frequency completely without removing the possibility of controlling the system.

I. INTRODUCTION

Superconducting quantum computers with moderate numbers of qubits are already available [1–5]. To increase the number of qubits further, every part of the current setups needs to be improved: data artificial atoms (AAs) that encode the qubits, room-temperature electronics that controls these AAs, and the interconnect between them. Simplifying this interconnect is the focus of this article. In particular, we show how to reduce the number of the needed transmission lines attached to each AA. The current designs [1–5] use separate lines for control and measurement of the AA. The control line is directly attached to the AA, but has a very small coupling such that the decay of the AA into this line is smaller than the other decoherence rates. The measurement line is coupled through a resonator that has a large detuning from the qubit transition frequency of the AA.

The measurement line is often filtered to suppress the decay of the AA into it. Such decay is conventionally called the “Purcell decay”, and the filters are called the “Purcell filters”. The Purcell filters are designed to break the trade-off between fast measurement and small decay rate into the measurement line by filtering the frequencies close to the qubit transition of the AA, but not the frequencies close to the frequency of the resonator [6, 7] [see Figs. 1(a) and 1(b)]. Other Purcell filter designs can be found in Refs. [8, 9]. Addition of an unsaturable Purcell filter to a transmission line makes it more challenging to control the AA, precisely due to the fact that the qubit frequency is filtered out. If this frequency is filtered out completely, a separate control line is required [1–5], but it is possible to make a trade-off be-

tween filtering and leaving a small coupling to perform control using the measurement line [9].

The qubit transition frequency could not be filtered out completely before the introduction of the Josephson quantum filter (JQF) [10, 11], which is another artificial atom. In the following, “AA” always means the data artificial atom that encodes the qubit, even though the JQF is also an artificial atom. The JQF matches the qubit transition of the AA (i.e., the transition frequencies of the two lowest energy levels are the same or close in AA and JQF), is strongly coupled to the control line, and is placed half a wavelength apart as shown in Fig. 1(c). When a strong control pulse is applied, the JQF becomes saturated and is effectively switched off. In the absence of the control pulses, the JQF prevents the decay at the qubit transition of the AA into the control line. Therefore, the JQF breaks the trade-off between fast control and small decay rate of the AA into the control line.

The contribution of this article is the realization that the JQF can also act as a Purcell filter when placed in the measurement line. Because the JQF can be saturated by strong control fields, it allows resonant control pulses to be sent in the measurement line, so that a separate control line is unnecessary. This results in the setup shown in Fig. 1(d). Because the control line is not directly attached to the AA, and due to the interference of the JQF, simple control pulses may not be sufficient to reach the extremely high gate fidelities needed for the fault-tolerant quantum computing [12]. Therefore, our results include the application of the quantum optimal control techniques that are compatible with the open system waveguide quantum electrodynamics setup that we consider.

Another way to decrease the number of the transmission lines is to use the frequency multiplexing [1–5, 7, 13–15]. Without the Purcell filters, both control and mea-

* ivan.las@tmd.ac.jp

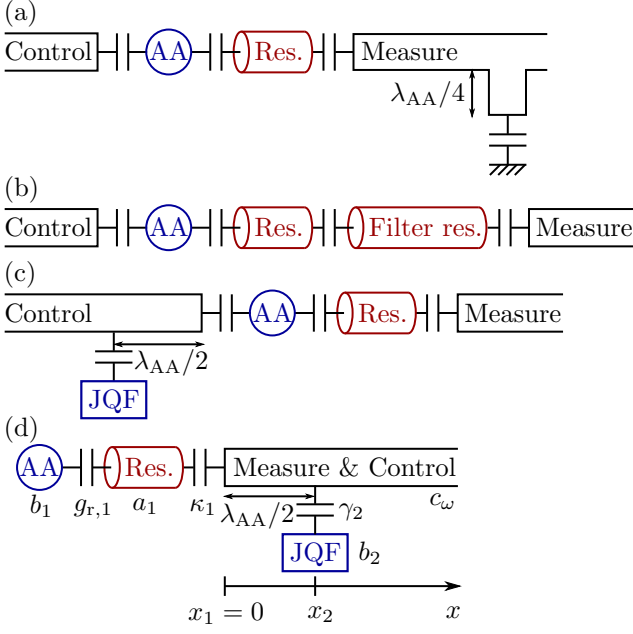


FIG. 1. (a) Band-rejection Purcell filtering of an artificial atom (AA) using a stub filter [6]. The measurement line is connected to the resonator (Res.) and has an open circuit stub with length $\lambda_{AA}/4$, where λ_{AA} is the wavelength corresponding to the qubit transition of the AA. An alternative design of a band-rejection filter can be found in Ref. [9]. (b) Band-pass Purcell filtering using a filter resonator [7]. The frequencies of the resonators are the same or close to each other. (c) Filtering of the control line using a Josephson quantum filter (JQF) [10, 11] placed $\lambda_{AA}/2$ away from the AA. The Purcell filter in the measurement line is not shown. (d) The setup that we consider—JQF as a saturable Purcell filter in the combined measurement and control line.

surement can be frequency multiplexed [13–15]. With the unsaturable Purcell filters, however, only the measurement is usually multiplexed [1–5, 7]. While the detailed investigation of the compatibility of JQFs as saturable Purcell filters and frequency multiplexing is out of scope for this article, such a combination would have the same low number of transmission lines as in Refs. [13–15], but with the Purcell filtering of the AAs.

Addition of Purcell filtering using a JQF could also be useful outside of the quantum computation context. E.g., in the hybrid systems setup of Ref. [16], the decoherence of the AA was found to be the main error source, to which the decay into the two transmission lines attached to the resonator was a major contribution. While the output transmission line could be filtered with an unsaturable Purcell filter, the input transmission line needs to pass through the control pulses for the AA, which is only possible to filter completely with a saturable Purcell filter such as a JQF.

The rest of the article is organized as follows. In Sec. II we set up the theoretical model and choose the parameters. In Sec. III, we show that the Purcell decay is sup-

pressed by the JQF. In Sec. IV, we show that the JQF does not disturb the measurement of the AA. In Sec. V, we show that AA can be controlled despite the presence of the JQF by finding the pulse shapes that implement a high-fidelity π -pulse. The article is concluded by Sec. VI.

II. SETUP

The considered setup is shown in Fig. 1(d). It consists of AA coupled to a single transmission line through a resonator, and a JQF coupled to the same line. The JQF is placed at the $\lambda_{AA}/2$ from the resonator, where λ_{AA} is the wavelength that corresponds to the transition frequency of the lowest two energy levels of the AA that encode the qubit. Both AA and JQF are assumed to be transmons, modeled as anharmonic oscillators. The model is set up for multiple AAs, resonators, and JQFs in view of a possible combination of the setup in Fig. 1(d) with the frequency multiplexing [13–15], but in this article we only analyze the setup in Fig. 1(d) in detail.

In the general case, there are M resonators with positions x_m , frequencies $\omega_{r,m}$, decay rates κ_m , and corresponding annihilation operators a_m . There are also N transmons (AAs and JQFs) with transition frequencies $\omega_{a,m}$ of the lowest two energy levels (which encode the qubit in the case of AA), anharmonicity parameters α_m , and corresponding annihilation operators b_m . Out of N transmons, M are coupled to the resonators with the coupling strength $g_{r,m}$. The other $N - M$ transmons are directly attached to the transmission line with positions x_m and decay rates γ_m . The annihilation operators c_ω of the transmission line correspond to the modes $\cos(k_\omega x)$ with positive wave vectors k_ω , but use the angular frequencies ω as the integration variable. The dispersion relation is $\omega = k_\omega v_g$, with v_g being the speed of light (group velocity) in the transmission line. The Hamiltonian can be written $H = H_f + H_i + H_s$. The transmission line field part is

$$H_f = \hbar \int_0^\infty \omega c_\omega^\dagger c_\omega d\omega; \quad (1)$$

the interaction part is

$$H_i = -\hbar \sum_{m=1}^N \int_0^\infty g_m(\omega) (c_\omega - c_\omega^\dagger) (\mathcal{O}_m - \mathcal{O}_m^\dagger) d\omega, \quad (2)$$

where $g_m(\omega) = G_m \sqrt{\omega} \cos(k_\omega x_m)$, $G_m = \sqrt{\Gamma_m / (2\pi\omega_m)}$,

$$\Gamma_m = \begin{cases} \kappa_m & \text{for } 1 \leq m \leq M, \\ \gamma_m & \text{for } M + 1 \leq m \leq N, \end{cases} \quad (3)$$

$$\omega_m = \begin{cases} \omega_{r,m} & \text{for } 1 \leq m \leq M, \\ \omega_{a,m} & \text{for } M + 1 \leq m \leq N, \end{cases} \quad (4)$$

$$\mathcal{O}_m = \begin{cases} a_m & \text{for } 1 \leq m \leq M, \\ b_m & \text{for } M + 1 \leq m \leq N; \end{cases} \quad (5)$$

the system part is $H_s = \sum_{m=1}^N H_{s,m}$, where

$$H_{s,m} = \hbar\omega_{a,m}b_m^\dagger b_m + \hbar\frac{\alpha_m}{2}(b_m^\dagger)^2 b_m^2 + \hbar\omega_{r,m}a_m^\dagger a_m + \hbar g_{r,m}(b_m^\dagger a_m + a_m^\dagger b_m) \quad (6)$$

for $1 \leq m \leq M$, and

$$H_{s,m} = \hbar\omega_{a,m}b_m^\dagger b_m + \hbar\frac{\alpha_m}{2}(b_m^\dagger)^2 b_m^2 \quad (7)$$

for $M+1 \leq m \leq N$. The rotating wave approximation is not applied immediately in H_i . It will be applied after the effective Heisenberg equations of motion for the subsystems (resonators, AAs, and JQFs) are obtained to ensure that all the terms are present [17]. More details about this can be found in App. A where the master equation is derived starting from the Hamiltonian above and following Refs. [10, 11, 17, 18]. Here, we only give the outline of this derivation.

Interaction of matter with electromagnetic fields results, in general, in non-Markovian equations of motion [19, 20] caused by the fact that it takes a finite time for the photons to propagate between the atoms. The effective equations of motion where the field degrees of freedom are traced out, take the form of the delay differential equations. The delay differential equations are difficult to solve in the general case, however, and hence some kind of approximation is usually needed. We adopt the approximation that converts the time delays into propagation phase factors [10, 11, 17, 18].

Before we explain this approximation, we first note that we diagonalize $H_{s,m}$ for every m . For every pair of eigenstates $|j_m\rangle, |j'_m\rangle$ of $H_{s,m}$, we define operators $\sigma_{m,jj'} = |j_m\rangle\langle j'_m|$ and matrix elements $C_{m,jj'} = \langle j_m|\mathcal{O}_m|j'_m\rangle$. We order the eigenstates such that the number of excitations increases or is constant with increasing j . Since \mathcal{O}_m is an annihilation operator, the rotating wave approximation ensures that $C_{m,jj'} \neq 0$ only for $j < j'$. We can write

$$H_{s,m} = \hbar \sum_j \omega_{m,j} \sigma_{m,jj}, \quad (8)$$

where $\omega_{m,j}$ are the eigenfrequencies.

Assuming that the Hamiltonian is dominated by the terms (8), the approximation of the delayed terms can be written

$$\sigma_{m,jj'}(t - t_x) \approx \sigma_{m,jj'}(t) e^{i(\omega_{m,j'} - \omega_{m,j})t_x}, \quad (9)$$

making the Heisenberg equations of motion for the N attached subsystems local in time. When a classical drive with frequency ω_d is present, we make the approximation

$$\sigma_{m,jj'}(t - t_x) \approx \sigma_{m,jj'}(t) e^{i\omega_d t_x} \quad (10)$$

instead. Physically, this means that the driven subsystems oscillate with the drive frequency rather than their eigenfrequencies.

The derivation assumes a coherent state with the carrier frequency ω_d as the input in the transmission line, and hence an additional drive Hamiltonian

$$H_d = \hbar \sum_{m=1}^N \left(\Omega_m e^{-i\omega_d t} \mathcal{O}_m^\dagger + (\Omega_m)^* e^{i\omega_d t} \mathcal{O}_m \right) \quad (11)$$

emerges with the Rabi frequencies

$$\Omega_m = \sqrt{\frac{\omega_d}{\omega_m} \Gamma_m \dot{n}} \cos(k_{\omega_d} x_m) e^{i\phi}, \quad (12)$$

which may be time-dependent due to the changing photon flux \dot{n} and phase ϕ .

The rotating frame is defined with respect to the Hamiltonian

$$H_0 = \hbar \sum_{m=1}^N \sum_j \omega_{0,m,j} \sigma_{m,jj}, \quad (13)$$

where frequencies $\omega_{0,m,j}$ are chosen such that the factors $e^{\pm i\omega_d t}$ in Eq. (11) are canceled, i.e., $\frac{i}{\hbar}[H_0, \mathcal{O}_m] = -i\omega_d \mathcal{O}_m$. If there is no drive, we choose $\frac{i}{\hbar}[H_0, \mathcal{O}_m] = -i\omega_{a,m_0} \mathcal{O}_m$ with $1 \leq m_0 \leq N$ instead. In the rotating frame with ω_d as the reference frequency, the Hamiltonian is

$$\tilde{H} = \hbar \sum_{m=1}^N \sum_j (\omega_{m,j} - \omega_{0,m,j}) \sigma_{m,jj} + \text{Re}[\Omega] \tilde{H}_{d,\text{Re}} + \text{Im}[\Omega] \tilde{H}_{d,\text{Im}}, \quad (14)$$

where we have picked one of the Rabi frequencies $\Omega = \Omega_{m_0}$ with $1 \leq m_0 \leq N$ as the reference one. Defining

$$\tilde{\Omega}_m = \frac{\text{Re}[\Omega_m]}{\text{Re}[\Omega]} = \frac{\text{Im}[\Omega_m]}{\text{Im}[\Omega]} = \sqrt{\frac{\omega_{m_0}}{\omega_m} \frac{\Gamma_m}{\Gamma_{m_0}} \cos(k_{\omega_d} x_m)}, \quad (15)$$

we can write

$$\tilde{H}_{d,\text{Re}} = \hbar \sum_{m=1}^N \tilde{\Omega}_m (\mathcal{O}_m^\dagger + \mathcal{O}_m), \quad (16a)$$

$$\tilde{H}_{d,\text{Im}} = i\hbar \sum_{m=1}^N \tilde{\Omega}_m (\mathcal{O}_m^\dagger - \mathcal{O}_m). \quad (16b)$$

The ratios $\tilde{\Omega}_m$ do not depend on the photon flux \dot{n} or phase ϕ , and hence $\tilde{H}_{d,\text{Re}}$ and $\tilde{H}_{d,\text{Im}}$ are independent of time. The time dependence of \tilde{H} is contained in the factors $\text{Re}[\Omega]$ and $\text{Im}[\Omega]$. The master equation can be written

$$\begin{aligned} \dot{\tilde{\rho}}_s &= \mathcal{L}(\tilde{\rho}_s) = -\frac{i}{\hbar} [\tilde{H}, \tilde{\rho}_s] \\ &+ \frac{1}{2} \sum_{m,n=1}^N (\mathcal{O}_{mn} \tilde{\rho}_s \mathcal{O}_m^\dagger - \mathcal{O}_m^\dagger \mathcal{O}_{mn} \tilde{\rho}_s) \\ &+ \frac{1}{2} \sum_{m,n=1}^N (\mathcal{O}_n \tilde{\rho}_s \mathcal{O}_{nm}^\dagger - \tilde{\rho}_s \mathcal{O}_{nm}^\dagger \mathcal{O}_n), \end{aligned} \quad (17)$$

where $\mathcal{O}_{mn} = \sum_{j,j'} \xi_{mn,j'j} C_{n,jj'} \sigma_{n,jj'}$,

$$\begin{aligned} \xi_{mn,j'j} &= \frac{\sqrt{\Gamma_m \Gamma_n}}{2} \frac{\omega_{n,j'j}}{\sqrt{\omega_m \omega_n}} \\ &\times \left(e^{ik_{n,j'j}|x_m - x_n|} + e^{ik_{n,j'j}|x_m + x_n|} \right), \end{aligned} \quad (18)$$

$\omega_{n,j'j} = \omega_{n,j'} - \omega_{n,j}$, $k_{n,j'j} = k_{\omega_{n,j'j}}$, and $\tilde{\rho}_s = e^{iH_0 t/\hbar} \text{tr}_t[\rho] e^{-iH_0 t/\hbar}$ is the density matrix with the transmission line field degrees of freedom traced out, in the rotating frame with respect to the Hamiltonian (13). If a classical drive is present, we set $k_{n,j'j} = k_{\omega_d}$ in Eq. (18), while keeping the factor $\omega_{n,j'j}/\sqrt{\omega_m \omega_n}$ unchanged.

The Schrieffer-Wolff transformation on the Hamiltonian (6) results in the dispersive shifts for every transmon energy level [21]. We define

$$\chi_m = \frac{g_{r,m}^2}{2(\omega_{r,m} - \omega_{a,m})} \left(1 - \frac{\omega_{r,m} - \omega_{a,m} + \alpha_m}{\omega_{r,m} - \omega_{a,m} - \alpha_m} \right) \quad (19)$$

in terms of the difference of the dispersive shifts for the lowest two levels. For $\alpha_m \rightarrow \infty$, this reduces to the two-level system shift $\chi_m = g_{r,m}^2 / (\omega_{r,m} - \omega_{a,m})$.

For the calculations below, we set the total number of subsystems $N = 2$, number of resonators $M = 1$, and the subsystem index is $m = 1, 2$. The parameters are chosen close to the ones in Ref. [11]. We set the frequency of the resonator $\omega_{r,1}/(2\pi) = 10$ GHz, resonator decay rate $\kappa_1/(2\pi) = 2$ MHz, transition frequencies of the lowest two energy levels of AA $\omega_{a,1}/(2\pi) = 8.000$ GHz and JQF $\omega_{a,2}/(2\pi) = 7.994$ GHz (shifted to match the frequency of the coupled eigenstate of AA and resonator), AA and JQF anharmonicities $\alpha_1/(2\pi) = \alpha_2/(2\pi) = -400$ MHz, JQF decay rate $\gamma_2/(2\pi) = 100$ MHz, and the dispersive shift between between AA and resonator $\chi_1/(2\pi) = 1$ MHz. Using Eq. (19), this sets the coupling between AA and resonator $g_{r,1}/(2\pi) = 109.544$ MHz. The resonator is placed at the origin, $x_1 = 0$, and the JQF is placed half a wavelength from the resonator, $k_{\omega_{a,1}} x_2 = \pi$. We also choose $\Omega = \Omega_1$ as the reference Rabi frequency, and hence $\tilde{\Omega}_1 = 1$ and $\tilde{\Omega}_2 = \sqrt{\omega_1 \gamma_2 / (\omega_2 \kappa_1)} \cos(k_{\omega_d} x_2)$.

III. SUPPRESSED PURCELL DECAY

First, we verify that the decay of a qubit stored in the subsystem with index $m = 1$ that consists of AA and resonator is reduced by adding a JQF (subsystem $m = 2$). The computational basis state $|0\rangle$ is defined to be the one where both the AA and the resonator are in their ground states, and therefore does not decay. The computational basis state $|1\rangle$ can be derived from the eigenvector of the matrix

$$\begin{pmatrix} \omega_{r,1} & g_{r,1} \\ g_{r,1} & \omega_{a,1} \end{pmatrix}, \quad (20)$$

which is the Hamiltonian (6) written in the single-excitation subspace spanned by the states $a_1^\dagger |0\rangle$ and $b_1^\dagger |0\rangle$.

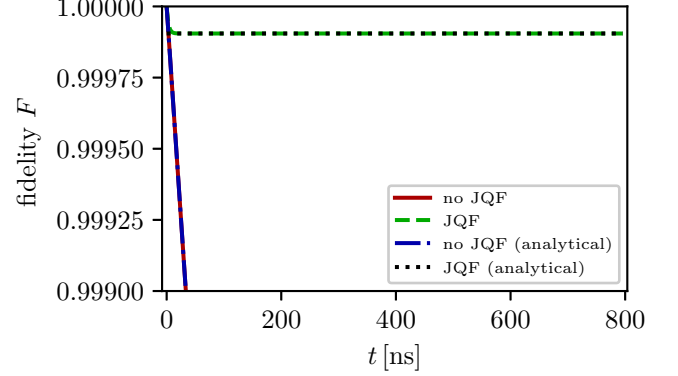


FIG. 2. Fidelity (23) as a function of time for the setup initialized in the state $|1\rangle = \sin(\theta)a_1^\dagger |0\rangle - \cos(\theta)b_1^\dagger |0\rangle$, where $\theta = \frac{1}{2} \arg[(\omega_{r,1} - \omega_{a,1})/2 + ig_{r,1}]$. The dash-dotted blue curve plots $e^{-\kappa_{\text{Purcell}} t}$ with κ_{Purcell} given by Eq. (21). The horizontal dotted black line plots F_{dark} given by Eq. (24). It overlaps the dashed green curve for large times.

We can write $|1\rangle = \sin(\theta)a_1^\dagger |0\rangle - \cos(\theta)b_1^\dagger |0\rangle$, where $\theta = \frac{1}{2} \arg[(\omega_{r,1} - \omega_{a,1})/2 + ig_{r,1}]$, and \arg is the argument of a complex number. As explained above, the Hamiltonian (6) for the subsystem consisting of AA and resonator is written in the diagonal form (8) prior to the derivation of the master equation (17). Hence, $|0\rangle = |j_1\rangle$ and $|1\rangle = |j'_1\rangle$ for some eigenstate indices j and j' . For a more straightforward notation below, we assume that $j = 0$ and $j' = 1$.

The decay of state $|1\rangle$ is suppressed by the large detuning of AA and resonator even without a JQF. From the master equation (17), the Purcell decay rate is

$$\kappa_{\text{Purcell}} = |C_{1,01}|^2 \xi_{11,10} = \sin^2(\theta) \kappa_1 \frac{\omega_{1,10}}{\omega_{r,1}}, \quad (21)$$

where $\omega_{1,10} = \omega_{1,1} - \omega_{1,0} = \omega_{1,1}$ and

$$\omega_{1,1} = \frac{\omega_{r,1} + \omega_{a,1}}{2} - \sqrt{\left(\frac{\omega_{r,1} - \omega_{a,1}}{2} \right)^2 + g_{r,1}^2}. \quad (22)$$

Since the detuning $\omega_{r,1} - \omega_{a,1}$ is large, we can approximate $\sin^2(\theta) \approx (g_{r,1}/(\omega_{r,1} - \omega_{a,1}))^2$, resulting in $\kappa_{\text{Purcell}} \approx (g_{r,1}/(\omega_{r,1} - \omega_{a,1}))^2 \kappa_1 (\omega_{1,10}/\omega_{r,1})$. The only difference from the usual formula for the Purcell decay rate is an additional factor $\omega_{1,10}/\omega_{r,1}$, which could be absorbed into the definition of the resonator decay rate κ_1 . For our parameters, $\omega_{1,10}/\omega_{r,1} = 0.7994$.

A Purcell filter needs to suppress the decay rate below κ_{Purcell} . We show in Fig. 2 that addition of a JQF accomplishes this. We initialize the AA and resonator system in state $|1\rangle$, and the JQF (if present) is initialized in its ground state. The plotted fidelity is given by

$$F = \text{tr}_s[(\sigma_{1,11} \otimes I_2) \tilde{\rho}_s(t)], \quad (23)$$

where tr_s is the trace over the system degrees of freedom (the trace over the transmission line degrees of freedom

tr_f has already been performed during the derivation of the master equation in App. A). We have also written the tensor product with the identity operator I_2 on the subsystem $m = 2$ (JQF) in Eq. (23) explicitly, so that it is more easily seen that $F = \langle 1 | \text{tr}_2(\tilde{\rho}_s) | 1 \rangle$, where tr_2 is the trace over the subsystem $m = 2$.

The solid red curve in Fig. 2 is the numerically calculated decay without a JQF, and the overlapping dash-dotted blue curve plots $e^{-\kappa_{\text{Purcell}} t}$. We see that the behavior of the dashed green curve that shows the case with a JQF is qualitatively the same as when the JQF was placed in the dedicated control line [10, 11]. Subsystem 1 (coupled AA and resonator) and subsystem 2 have both bright states that decay rapidly and dark states that do not decay. The state, where AA and resonator are in the computational basis state $|1\rangle$ and the JQF is in the ground state, has bright and dark parts. Because the coupling of the JQF to the transmission line is significantly larger, this state is mostly dark. After the rapid decay of the small bright part, the decay rate vanishes due to the fact that our model does not have other sources of decoherence besides the decay caused by the coupling to the transmission line. The fidelity after the bright part has decayed is

$$F_{\text{dark}} = \left(\frac{\gamma_2}{\kappa_{\text{Purcell}} + \gamma_2} \right)^2, \quad (24)$$

shown as the horizontal dotted black line in Fig. 2.

In practice, other sources of decoherence will be present, and hence the decay rate is not expected to be zero but still be reduced compared to the case without a JQF, similar to the experimental implementation of the JQF in the control line [11]. We also note that the JQF transition frequency is chosen to match the eigenfrequency of state $|1\rangle$, i.e., $\omega_{a,2}/(2\pi) = \omega_{1,1}/(2\pi) = 7.994$ GHz, and other frequencies of the JQF give an imperfect decay rate cancellation, as shown in Fig. 3.

In App. B, we numerically show that the approximation (9) used in the derivation of the master equation (17) is responsible for the unphysical result where the decay rate becomes negative (i.e., fidelity increases with time). This is the case for the dashed green curve in Fig. (2), but requires a significant zoom factor to be seen. Not performing the approximation (9) results in the delay differential equations, which can be solved for the single-excitation subspace. This gives a modification of the “steady-state” value of the dashed green curve in Fig. (2) and a small positive long-time decay rate, as expected on physical grounds. Therefore, it is possible to estimate the fidelity error due to the approximation (9), putting it around $2 \cdot 10^{-6}$.

IV. REFLECTED PHASE

When the resonator is probed by a resonant probe field ($\omega_d \approx \omega_{r,1}$), the phase of the reflected field is different

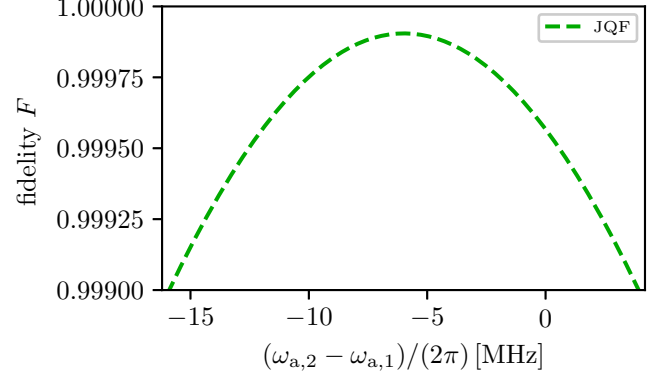


FIG. 3. Fidelity (23) as a function of JQF transition frequency $\omega_{a,2}$ for the setup that was initialized in the state $|1\rangle$ and decayed for same time $t_f = 10/\kappa_1 \approx 800$ ns as in Fig. 2, plotting the final value. The parameters are the same as in Fig. 2, except for $\omega_{a,2}$.

for states $|0\rangle$ and $|1\rangle$, and this is the standard physical mechanism for state measurement in the superconducting quantum computers [1–5, 7]. While the theoretical description of this measurement mechanism could be made more advanced [22, 23], we take the simple approach of only considering the expectation value of the reflected phase. Since the JQF is far detuned from the probe (around 2 GHz in our assumed parameters), it is weakly excited even for moderate powers of the probing field, and therefore the noise contribution is assumed to be negligible. In this case, only the expectation values of the reflected phase need to be examined. The argument is the following: if the measurement works without the JQF, and the JQF does not significantly modify the expectation values of the reflected phase, then the measurement is expected to work with the JQF.

In App. C, we derive the expression for the reflection coefficient

$$r = 1 - i \sum_{m=1}^N \sum_{j,j'} \frac{\omega_{m,j'j}}{\sqrt{\omega_1 \omega_m}} \frac{\sqrt{\Gamma_1 \Gamma_m}}{\Omega_1} C_{m,jj'} \times \text{tr}_s[\sigma_{m,jj'} \tilde{\rho}_s] \cos(k_{\omega_d} x_m) \quad (25)$$

at the position $x_N^+ = x_N + \epsilon$ for $\epsilon \rightarrow 0$ from above, i.e., just to the right of the last subsystem attached to the transmission line (the JQF). The expression is written in terms of the reference Rabi frequency Ω_1 , and the overall propagation phase $e^{2ik_{\omega_d} x_N^+}$ has been removed. The master equation (17) is solved to evaluate the expectation values $\text{tr}_s[\sigma_{m,jj'} \tilde{\rho}_s]$, and the reflection coefficient as a function of time is calculated. The true steady-state reflection coefficient for both of the two initial states, $|0\rangle$ and $|1\rangle$, is the same since state $|1\rangle$ eventually decays into state $|0\rangle$. Therefore, we evolve the master equation for a finite time, which is long enough for the transients to disappear, but short enough that state $|1\rangle$ does not decay significantly. We choose evolution time $t_f = 20/\kappa_1 \approx 1.6 \mu\text{s}$ in Fig. 4,

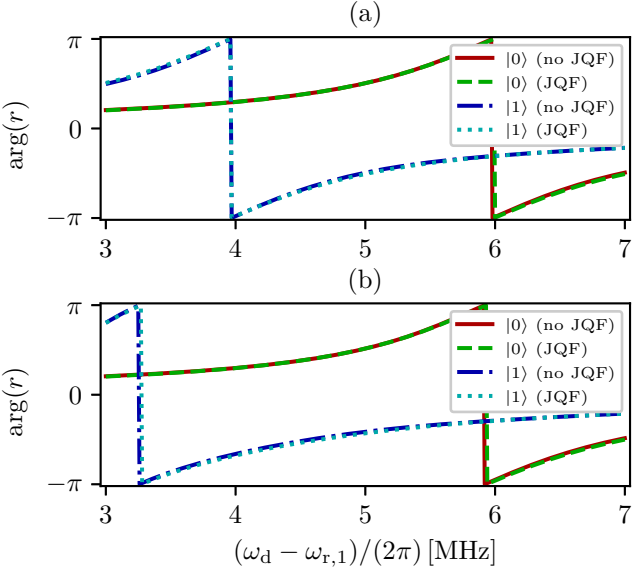


FIG. 4. The phase of the reflection coefficient (25) as a function of the probe frequency ω_d for Rabi frequencies of the probe: (a) $\Omega_1/(2\pi) = 1$ MHz, (b) $\Omega_1/(2\pi) = 4$ MHz. In both cases, the setup is initialized either in state $|0\rangle$ or state $|1\rangle$, and the curves with and without the JQF are shown.

where we plot the reflected phase.

We consider two different probe Rabi frequencies, $\Omega_1/(2\pi) = 1$ MHz and $\Omega_1/(2\pi) = 4$ MHz [Fig. 4(a) and Fig. 4(b), respectively]. The former corresponds to -137 dBm [cf. Eq. (12)] and is chosen to have one photon on average inside an empty resonator that is probed on resonance ($\omega_d = \omega_{r,1}$) without a JQF in front. The latter Rabi frequency corresponds to -125 dBm and results in 16 photons on average in the same empty resonator setup. These average populations are modified slightly due to the addition of AA and JQF. While Figs. 4(a) and 4(b) illustrate the response of the AA and resonator system to different probe powers, both show that the change of the expectation value of the reflected phase due to presence of the JQF is negligible. Hence, by the discussion above, the state measurement should not be affected by the JQF.

V. CONTROL

To verify the controllability of the system despite the complications arising from coupling to AA through a JQF and a resonator, we show that the state of the system can be transferred from state $|0\rangle$ to state $|1\rangle$ with high fidelity. For a two-level atom with a directly attached control line, this can be accomplished with a simple rectangular pulse. The setup where the two-level atom is replaced with a transmon and JQF added in the control line [Fig. 1(c)] requires pulses that are more carefully chosen [11, 24]. For the setup that we are

considering here [Fig. 1(d)], we choose a more general parametrization of the pulses, inspired by Refs. [25–27], but with a different way to calculate the gradient, as explained below.

We set the carrier frequency of the drive equal to the transition frequency of coupled eigenstate of AA and resonator $|1\rangle$ ($\omega_d = \omega_{1,1} = \omega_{a,2}$) and parametrize the time-dependent Rabi frequencies as Gaussian-filtered Fourier series to limit the bandwidth. The minimum and maximum values are constrained by applying the tanh function. We can write this parametrization

$$\text{Re}[\Omega](t) = \Omega_{\max} \tanh \left(w(t) \sum_{p=1}^{N_c} a_p f_p(t) \right), \quad (26a)$$

$$\text{Im}[\Omega](t) = \Omega_{\max} \tanh \left(w(t) \sum_{p=1}^{N_c} b_p f_p(t) \right), \quad (26b)$$

where Ω_{\max} is the maximum absolute value of the real and imaginary components of the Rabi frequency, N_c is the maximum number of the Fourier terms,

$$f_p(t) = \frac{1}{\sigma_f \sqrt{\pi t_f}} \int_0^{t_f} \exp \left(-\frac{(t-t')^2}{2\sigma_f^2} \right) \sin(\omega_p t') dt', \quad (27)$$

$\omega_p = p\pi/t_f$, w is a confined Gaussian window function [28] that fulfills $w(0) = w(t_f) = 0$. Without filtering, we have $\sin(0) = \sin(\omega_p t_f) = 0$ by construction, but this is no longer true for the filtered f_p , and therefore an additional window function was used. Expressions for $f_p(t)$ and $w(t)$ can be found in App. D. The analytical expression for $f_p(t)$ was found not to be numerically stable for large p . Instead, we calculate $f_p(t)$ by the numerical integration [29] of Eq. (27).

Starting in state $|0\rangle$, we maximize the fidelity

$$\tilde{F} = \text{tr}_s[(\sigma_{1,11} \otimes \sigma_{2,00}) \tilde{\rho}_s(t)], \quad (28)$$

at the final time $t = t_f$ as a function of the Fourier coefficients a_p and b_p . Compared to the fidelity F given by Eq. (23), the trace over the JQF is not performed, requiring it to be in the ground state $|0_2\rangle$ at the end of the π -pulse. This is to ensure that the JQF does not disturb the state of AA by emitting a photon after the π -pulse is performed. The master equation (17) is be rewritten such that the elements of the density matrix $\tilde{\rho}_s$ are arranged as a vector $\tilde{\rho}_s$, resulting in $\tilde{\rho}_s = L(t)\tilde{\rho}_s$. In the same way, the matrix $M_{\tilde{F}} = \sigma_{1,11} \otimes \sigma_{2,00}$ is also written as a vector $\tilde{M}_{\tilde{F}}$, and hence we can write Eq. (28) as an inner product

$$\tilde{F} = \tilde{M}_{\tilde{F}}^\dagger \tilde{\rho}_s(t). \quad (29)$$

We solve the master equation with the 4th order Runge-Kutta method and use the reverse mode automatic differentiation to calculate the gradient of Eq. (29)

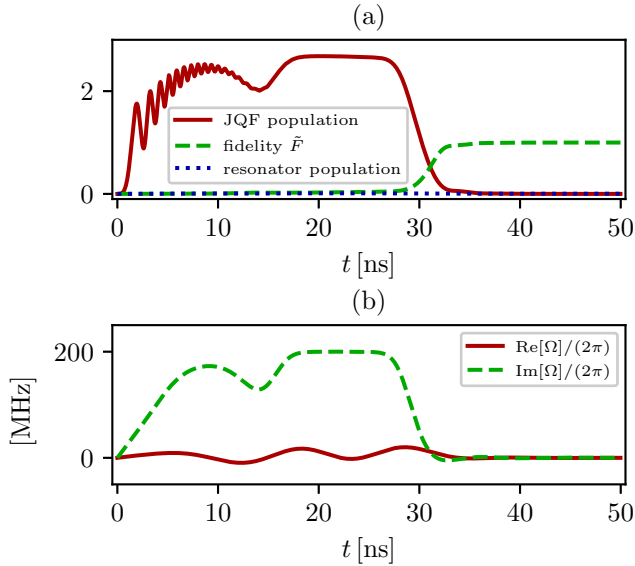


FIG. 5. (a) Fidelity (28), resonator population $\langle a_1^\dagger a_1 \rangle$, and JQF population $\langle b_2^\dagger b_2 \rangle$ as functions of time for the setup initialized in state $|0\rangle$ and driven to state $|1\rangle$ by the time-dependent Rabi frequency shown in (b). The achieved π -pulse fidelity is $\tilde{F} = 0.9993$. The number of Fourier components in the parametrization (26) is $N_c = 100$ (for each of $\text{Re}[\Omega]$ and $\text{Im}[\Omega]$). The functions (27) are filtered with $\sigma_f = 0.1/\kappa$, corresponding to the bandwidth $1/\sigma_f \approx 126$ MHz. The window function w uses $\sigma_w = 0.1t_f$ [cf. Eq. (D3)]. The maximum Rabi frequency is set to $\Omega_{\max}/(2\pi) = 200$ MHz, corresponding to -91 dBm [cf. Eq. (12)].

with respect to the Fourier components a_p and b_p . Compared to the general case of non-linear differential equations solved by the Runge-Kutta method [30, 31], the linearity of the master equation allows for an approach that is superficially similar to the other optimal control approaches where forward propagation of the equations of motion is alternated with backward propagation of the adjoint equations [32, 33]. In contrast to Refs. [32, 33], however, the derivation of the adjoint equation is more involved than simply taking the adjoint of $L(t)$, as explained in App. D. The calculated gradients are then used together with the LBFGS algorithm [34, 35] to find the maximum of \tilde{F} . The resulting evolution of \tilde{F} and populations of the resonator and JQF is shown in Fig. 5(a). The corresponding time-dependent Rabi frequency is shown in Fig. 5(b).

As we see in Fig. 5(a), the JQF is driven to higher excitation levels by the strong control fields and hence is effectively decoupled from the transmission line, permitting control of AA. Nevertheless, the JQF is emitting off-resonant photons during this time, affecting the evolution of AA in a nontrivial way. While we do not have any intuition about what needs to be done to cancel these nonlinear effects, the chosen optimal control method is sufficient to account for this, reaching a high fidelity

$\tilde{F} = 0.9993$. The choices of the 50 ns gate time and the required bandwidth $1/\sigma_f \approx 126$ MHz are conservative. If the gate time is decreased, the fidelity decreases, but a larger bandwidth and amplitude of the pulses can enable high fidelity even for small gate times. Since it is possible to synthesize microwave pulses with bandwidths of several GHz [36, 37], there is room for improvement for both the gate time and fidelity.

VI. CONCLUSION

We have shown theoretically that it is possible to construct a saturable Purcell filter using an artificial atom directly attached to the transmission line. This filter suppresses the Purcell decay when the control fields are absent and can be effectively switched off by saturation when the control fields are present. This allows both the control and measurement of the data artificial atom to be performed using a single transmission line while maintaining long coherence time. Our results can be used to decrease the number of needed transmission lines in superconducting quantum computers and other setups involving superconducting artificial atoms. Further reductions in the number of transmission lines could be achieved by combining saturable Purcell filters with the frequency multiplexing.

ACKNOWLEDGMENTS

The authors acknowledge T. Shitara, S. Goto, and Y. Sunada for fruitful discussions. This work was supported by JST ERATO (Grant No. JPMJER1601), JST Moonshot R&D (Grant Nos. JPMJMS2067-3 and JPMJMS2061-2-1-2), and JSPS KAKENHI (Grant No. 19K03684).

Appendix A: Derivation of the master equation

In this appendix, we derive the master equation (17), following Refs. [10, 11, 17, 18]. The Heisenberg equations of motion for the field operators are

$$\dot{c}_\omega = -i\omega c_\omega - i \sum_{m=1}^N g_m(\omega) (\mathcal{O}_m - \mathcal{O}_m^\dagger) \quad (\text{A1})$$

with the solutions

$$c_\omega = c_\omega(0) e^{-i\omega t} - i \sum_{m=1}^N g_m(\omega) \times \int_0^t (\mathcal{O}_m(t-t') - \mathcal{O}_m^\dagger(t-t')) e^{-i\omega t'} dt'. \quad (\text{A2})$$

Here and below, the indication of the time-dependence of the operators is omitted for brevity as long as it is of the

simple form: c_ω means $c_\omega(t)$ in the above expressions. Note that the term involving \mathcal{O}_m^\dagger is present, because the rotating wave approximation is *not* performed [17] in the Hamiltonian (2). Once we calculate

$$\begin{aligned} c_\omega - c_\omega^\dagger &= c_\omega(0)e^{-i\omega t} - c_\omega^\dagger(0)e^{i\omega t} - i \sum_{m=1}^N g_m(\omega) \\ &\times \left(\int_0^t \mathcal{O}_m(t-t') \left(e^{-i\omega t'} - e^{i\omega t'} \right) dt' \right. \\ &\left. - \int_0^t \mathcal{O}_m^\dagger(t-t') \left(e^{-i\omega t'} - e^{i\omega t'} \right) dt' \right), \end{aligned} \quad (\text{A3})$$

we see that terms arising from not performing the rotating wave approximation appear as additional $e^{\pm i\omega t'}$ in the inner parentheses. These will allow us to extend the integrations over ω to the entire real line.

The expression for $c_\omega - c_\omega^\dagger$ is needed in the Heisenberg equation of motion for an arbitrary system operator Q ,

$$\begin{aligned} \dot{Q} &= \frac{i}{\hbar} [H_s, Q] + i \sum_{m=1}^N \int_0^\infty g_m(\omega) \\ &\times \left([\mathcal{O}_m^\dagger, Q](c_\omega - c_\omega^\dagger) - (c_\omega - c_\omega^\dagger)[\mathcal{O}_m, Q] \right) d\omega, \end{aligned} \quad (\text{A4})$$

written in the normal ordered form. When we insert Eq. (A3), the normal ordering becomes important. The integrations over ω are carried out first. We have

$$\begin{aligned} &\int_0^\infty g_m(\omega) g_n(\omega) \left(e^{-i\omega t'} - e^{i\omega t'} \right) d\omega \\ &= \frac{i\pi G_m G_n}{2} \left(\dot{\delta} \left(t' - \frac{x_m - x_n}{v_g} \right) + \dot{\delta} \left(t' + \frac{x_m - x_n}{v_g} \right) \right. \\ &\left. + \dot{\delta} \left(t' - \frac{x_m + x_n}{v_g} \right) + \dot{\delta} \left(t' + \frac{x_m + x_n}{v_g} \right) \right), \end{aligned} \quad (\text{A5})$$

where $\dot{\delta}$ is the derivative of the Dirac delta function that has the property

$$\int_0^t \dot{\delta}(t' - t_x) f(t - t') dt' = \dot{f}(t - t_x), \quad (\text{A6})$$

as long as $0 < t_x < t$, where f is an arbitrary (operator-valued) function, and the integration limits are chosen as to be relevant to the present derivation. The case with $t_x = 0$ is defined with $\dot{f}(t)/2$ on the right hand side of Eq. (A6). Since $t_x = 0$ is equivalent to $x_m, x_n = 0$ in Eq. (A5), this case could also be addressed by setting $x_m, x_n = 0$ in the integral on the left hand side of Eq. (A5). Thus,

$$\begin{aligned} &\int_0^t \left(\dot{\delta} \left(t' - \frac{x_m \pm x_n}{v_g} \right) + \dot{\delta} \left(t' + \frac{x_m \pm x_n}{v_g} \right) \right) \\ &\times \mathcal{O}_n(t - t') dt' \\ &= \dot{\mathcal{O}}_n \left(t - \frac{|x_m \pm x_n|}{v_g} \right) \theta_H \left(t - \frac{|x_m \pm x_n|}{v_g} \right), \end{aligned} \quad (\text{A7})$$

where θ_H is the Heaviside theta function.

Defining the noise operator

$$\mathcal{N}_m = \int_0^\infty g_m(\omega) c_\omega(0) e^{-i\omega t} d\omega, \quad (\text{A8})$$

and applying the rotating wave approximation, we can write

$$\begin{aligned} \dot{Q} &= \frac{i}{\hbar} [H_s, Q] + i \sum_{m=1}^N \left([\mathcal{O}_m^\dagger, Q] \mathcal{N}_m + \mathcal{N}_m^\dagger [\mathcal{O}_m, Q] \right) \\ &+ \sum_{m,n=1}^N \frac{i\pi G_m G_n}{2} [\mathcal{O}_m^\dagger, Q] \left(\dot{\mathcal{O}}_n \left(t - \frac{|x_m - x_n|}{v_g} \right) \right. \\ &\left. + \dot{\mathcal{O}}_n \left(t - \frac{|x_m + x_n|}{v_g} \right) \right) \\ &+ \sum_{m,n=1}^N \frac{i\pi G_m G_n}{2} \left(\dot{\mathcal{O}}_n^\dagger \left(t - \frac{|x_m - x_n|}{v_g} \right) \right. \\ &\left. + \dot{\mathcal{O}}_n^\dagger \left(t - \frac{|x_m + x_n|}{v_g} \right) \right) [\mathcal{O}_m, Q], \end{aligned} \quad (\text{A9})$$

where the Heaviside theta function factors resulting from Eq. (A7) are implicit. We make one more approximation by setting

$$\dot{\mathcal{O}}_n(t - t_x) \approx -i \sum_{j,j'} \omega_{n,j'j} C_{n,jj'} \sigma_{n,jj'}(t - t_x), \quad (\text{A10})$$

where $\omega_{n,j'j} = \omega_{n,j'} - \omega_{n,j}$. This approximation can be viewed as applying Eq. (A9) and ignoring all the terms besides $\frac{i}{\hbar} [H_s, \mathcal{O}_n]$ due to the fact that the absolute frequencies $\omega_{n,j'j}$ are large compared to the couplings G_n . Thus, this is also a form of a rotating wave approximation.

In App. B, equations of motion in the single-excitation subspace are derived from Eq. (A9) without any further approximations besides Eq. (A10). For the master equation (17), Eq. (A9) needs to be approximated such that it becomes local in time, i.e. does not contain operators at previous times $t - |x_m \pm x_n|/v_g$. We use either approximation (9) or (10) together with the approximation (A10). Additionally, we assume that the size of the ensemble is small, i.e., $|x_m \pm x_n|/v_g$ is short compared to the time scales of interest, and hence we set $\theta_H(t - |x_m \pm x_n|/v_g) = 1$ for all t .

Using the approximation (9), inserting $G_m = \sqrt{\Gamma_m/(2\pi\omega_m)}$, identifying $\xi_{mn,j'j}$ given by Eq. (18) and $\mathcal{O}_{mn} = \sum_{j,j'} \xi_{mn,j'j} C_{n,jj'} \sigma_{n,jj'}$, we get

$$\begin{aligned} \dot{Q} &= \frac{i}{\hbar} [H_s, Q] + i \sum_{m=1}^N \left([\mathcal{O}_m^\dagger, Q] \mathcal{N}_m + \mathcal{N}_m^\dagger [\mathcal{O}_m, Q] \right) \\ &+ \frac{1}{2} \sum_{m,n=1}^N \left([\mathcal{O}_m^\dagger, Q] \mathcal{O}_{mn} - \mathcal{O}_{mn}^\dagger [\mathcal{O}_m, Q] \right). \end{aligned} \quad (\text{A11})$$

The above equation with the drive approximation (10) is obtained by setting $k_{n,j'j} = k_{\omega_d}$ in Eq. (18).

Since the expectation values are the same in the Heisenberg and Schrödinger pictures, we have

$$\langle Q \rangle = \text{tr}_s \text{tr}_f [Q \rho(0)] = \text{tr}_s [Q(0) \rho_s], \quad (\text{A12})$$

where tr_s (tr_f) is the trace over the system (field) degrees of freedom, and $\rho_s = \text{tr}_f[\rho]$. Taking the time derivative, we get

$$\text{tr}_s \text{tr}_f [\dot{Q} \rho(0)] = \text{tr}_s [Q(0) \dot{\rho}_s]. \quad (\text{A13})$$

The procedure to obtain the master equation (17) starts with inserting Eq. (A11) into the left hand side of Eq. (A13). The resulting expression can then be rewritten in the form $\text{tr}_s [Q(0)B]$, where B is some system operator expression. Using the right hand side of Eq. (A13), the master equation is obtained as $\dot{\rho}_s = B$.

For any system operator A ,

$$\text{tr}_s \text{tr}_f [[A, Q] \rho(0)] = -\text{tr}_s [Q(0) [A(0), \rho_s]]. \quad (\text{A14})$$

In $\text{tr}_s \text{tr}_f [[\mathcal{O}_m^\dagger, Q] \mathcal{N}_m \rho(0)]$ and $\text{tr}_s \text{tr}_f [\mathcal{N}_m^\dagger [\mathcal{O}_m, Q] \rho(0)]$, we assume that $\rho(0) = \rho_s(0) \otimes \rho_f(0)$ with the state of the field $\rho_f(0) = |\{\alpha_\omega\}\rangle\langle\{\alpha_\omega\}|$ being a multimode coherent state. This state could be written as the displaced vacuum state $|\{\alpha_\omega\}\rangle = D(\{\alpha_\omega\})|\text{vac}\rangle$, where the displacement operator is

$$D(\{\alpha_\omega\}) = \exp \left(\int_0^\infty (\alpha_\omega c_\omega^\dagger(0) - \alpha_\omega^* c_\omega(0)) d\omega \right). \quad (\text{A15})$$

We have

$$c_\omega(0) |\{\alpha_\omega\}\rangle = \alpha_\omega |\{\alpha_\omega\}\rangle. \quad (\text{A16})$$

To relate α_ω to the photon flux \dot{n} , we define Fourier transformed operators [38]

$$c_t = \frac{1}{\sqrt{2\pi}} \int_0^\infty c_\omega(0) e^{-i\omega t} d\omega, \quad (\text{A17})$$

and then the photon flux is $\dot{n} = \langle c_t^\dagger c_t \rangle = |\alpha_t|^2$, where

$$\alpha_t = \frac{1}{\sqrt{2\pi}} \int_0^\infty \alpha_\omega e^{-i\omega t} d\omega. \quad (\text{A18})$$

For the operators (A8), it holds that

$$\mathcal{N}_m |\{\alpha_\omega\}\rangle = \Omega_m e^{-i\omega_d t} |\{\alpha_\omega\}\rangle, \quad (\text{A19})$$

where we have defined the Rabi frequency

$$\Omega_m e^{-i\omega_d t} = \int_0^\infty g_m(\omega) \alpha_\omega e^{-i\omega t} d\omega. \quad (\text{A20})$$

To go from Eq. (A20) to Eq. (12), a narrow-bandwidth approximation is made, $g_m(\omega) \approx g_m(\omega_d)$, resulting in $\Omega_m e^{-i\omega_d t} = \sqrt{2\pi} g_m(\omega_d) \alpha_t$. Since $\dot{n} = |\alpha_t|^2$, we set $\alpha_t = \sqrt{\dot{n}} e^{-i\omega_d t} e^{i\phi}$ for some phase ϕ , and then Eq. (12)

is obtained. For the reflection coefficient calculations [Sec. IV and App. C], we also need to consider the case of the infinitely narrow bandwidth continuous wave input, where

$$c_\omega(0) |\{\alpha_\omega\}\rangle = \sqrt{2\pi \dot{n}} e^{i\phi} \delta(\omega - \omega_d) |\{\alpha_\omega\}\rangle. \quad (\text{A21})$$

Using Eq. (A19), the terms $\text{tr}_s \text{tr}_f [[\mathcal{O}_m^\dagger, Q] \mathcal{N}_m \rho(0)]$ and $\text{tr}_s \text{tr}_f [\mathcal{N}_m^\dagger [\mathcal{O}_m, Q] \rho(0)]$ are simplified into the form where Eq. (A14) can be applied. These terms give rise to the drive Hamiltonian (11). Together with the other terms rewritten either using either Eq. (A14) or in a similar way, we get the master equation

$$\begin{aligned} \dot{\rho}_s = & -\frac{i}{\hbar} [H_d + H_s, \rho_s] \\ & + \frac{1}{2} \sum_{m,n=1}^N \left(\mathcal{O}_{mn} \rho_s \mathcal{O}_m^\dagger - \mathcal{O}_m^\dagger \mathcal{O}_{mn} \rho_s \right) \\ & + \frac{1}{2} \sum_{m,n=1}^N \left(\mathcal{O}_n \rho_s \mathcal{O}_{nm}^\dagger - \rho_s \mathcal{O}_{nm}^\dagger \mathcal{O}_n \right). \end{aligned} \quad (\text{A22})$$

Transforming Eq. (A22) into the rotating frame with respect to the Hamiltonian (13) by substituting $\rho_s = e^{-iH_0 t/\hbar} \tilde{\rho}_s e^{iH_0 t/\hbar}$ results in the master equation (17) with

$$\tilde{H} = e^{iH_0 t/\hbar} (H_d + H_s) e^{-iH_0 t/\hbar} - H_0. \quad (\text{A23})$$

Frequencies $\omega_{0,m,j}$ in Eq. (13) are chosen such that $\frac{i}{\hbar} [H_0, \mathcal{O}_m] = -i\omega_d \mathcal{O}_m$, and thus the factors $e^{\pm i\omega_d t}$ in Eq. (11) are canceled. By inserting $\mathcal{O}_m = C_{m,j,j'} \sigma_{m,j,j'}$, the equivalent condition is

$$\omega_{0,m,j'} - \omega_{0,m,j} = \omega_d \quad (\text{A24})$$

for every $C_{m,j,j'} \neq 0$. It is possible to satisfy this condition, since \mathcal{O}_m is an annihilation operator, and hence $C_{m,j,j'} \neq 0$ only if j and j' correspond to the eigenstates with excitation numbers $N_{m,j}$ and $N_{m,j'} = N_{m,j} + 1$, respectively. Thus, setting $\omega_{0,m,j} = N_{m,j} \omega_d$ satisfies Eq. (A24). With this choice, Eq. (A23) becomes Eq. (14).

Appendix B: Delay differential equations for the decay

In this appendix, we derive the model for the decay without the approximations (9) or (10) following the approach of Ref. [10]. In the single-excitation subspace, only 3 subsystem states are relevant: a single excitation in either AA, resonator, or JQF. Using the diagonal basis, the subsystem of AA and resonator is represented by the two eigenstates

$$|1_1\rangle = \sin(\theta) a_1^\dagger |0_1\rangle - \cos(\theta) b_1^\dagger |0_1\rangle, \quad (\text{B1a})$$

$$|2_1\rangle = \cos(\theta) a_1^\dagger |0_1\rangle + \sin(\theta) b_1^\dagger |0_1\rangle, \quad (\text{B1b})$$

where $\theta = \frac{1}{2} \arg[(\omega_{r,1} - \omega_{a,1})/2 + i g_{r,1}]$. Eigenstates $|0_1\rangle$ and $|1_1\rangle$ are the same as the computational basis states

$|0\rangle$ and $|1\rangle$ used in the main text, while $|2_1\rangle$ is the rapidly-decaying eigenstate with most of the excitation in the resonator. The eigenfrequency corresponding to state $|1\rangle$ is given by Eq. (22), and eigenfrequency corresponding to state $|2_1\rangle$ is

$$\omega_{1,2} = \frac{\omega_{r,1} + \omega_{a,1}}{2} + \sqrt{\left(\frac{\omega_{r,1} - \omega_{a,1}}{2}\right)^2 + g_{r,1}^2}. \quad (\text{B2})$$

For the JQF, there is only one eigenstate $|1_2\rangle$ to consider. In the single-excitation subspace, we therefore have

$$\mathcal{O}_1 = a_1 = C_{1,01}\sigma_{1,01} + C_{1,02}\sigma_{1,02}, \quad (\text{B3a})$$

$$\mathcal{O}_2 = b_2 = C_{2,01}\sigma_{2,01}, \quad (\text{B3b})$$

where $C_{1,01} = \langle 0_1 | a_1 | 1_1 \rangle = \sin(\theta)$, $C_{1,02} = \langle 0_1 | a_1 | 2_1 \rangle = \cos(\theta)$, and $C_{2,01} = \langle 0_2 | b_2 | 1_2 \rangle = 1$.

Equations of motion for the operators $\sigma_{m,0j}$ are obtained from Eq. (A9) under the approximation (A10).

We consider the single-excitation state

$$|\psi(t)\rangle = \sum_{m,j} \alpha_{m,j}(t) \sigma_{m,j0}(0) |\text{vac}\rangle + \int_0^\infty f_\omega(t) c_\omega^\dagger(0) d\omega |\text{vac}\rangle, \quad (\text{B4})$$

where $|\text{vac}\rangle = |0_1\rangle|0_2\rangle|\text{vac}_c\rangle$, and $|\text{vac}_c\rangle$ is the vacuum state for the transmission line. The equations of motion for the amplitudes $\alpha_{m,j}$ are found as

$$\dot{\alpha}_{m,j}(t) = \langle \text{vac} | \dot{\sigma}_{m,0j}(t) | \psi(0) \rangle. \quad (\text{B5})$$

Defining the inputs $f_{\text{in},m}(t) = \int_0^\infty g_m(\omega) f_\omega(0) e^{-i\omega t} d\omega$, slowly-varying quantities $\alpha_{m,j}(t) = \tilde{\alpha}_{m,j}(t) e^{-i\omega_{a,1} t}$ and $f_{\text{in},m}(t) = \tilde{f}_{\text{in},m}(t) e^{-i\omega_{a,1} t}$, and setting $x_1 = 0$ for simplicity, gives the delay differential equations

$$\begin{aligned} \dot{\tilde{\alpha}}_{1,1}(t) = & -i(\omega_{1,10} - \omega_{a,1})\tilde{\alpha}_{1,1}(t) - iC_{1,01}^* \tilde{f}_{\text{in},1}(t) - |C_{1,01}|^2 \frac{\kappa_1}{2} \frac{\omega_{1,10}}{\omega_{r,1}} \tilde{\alpha}_{1,1}(t) - C_{1,01}^* C_{1,02} \frac{\kappa_1}{2} \frac{\omega_{1,20}}{\omega_{r,1}} \tilde{\alpha}_{1,2}(t) \\ & - C_{1,01}^* C_{2,01} \frac{\sqrt{\kappa_1 \gamma_2}}{2} \frac{\omega_{2,10}}{\sqrt{\omega_{r,1} \omega_{a,2}}} e^{ik_{a,1} x_2} \tilde{\alpha}_{2,1}(t - x_2/v_g), \end{aligned} \quad (\text{B6a})$$

$$\begin{aligned} \dot{\tilde{\alpha}}_{1,2}(t) = & -i(\omega_{1,20} - \omega_{a,1})\tilde{\alpha}_{1,2}(t) - iC_{1,02}^* \tilde{f}_{\text{in},1}(t) - |C_{1,02}|^2 \frac{\kappa_1}{2} \frac{\omega_{1,20}}{\omega_{r,1}} \tilde{\alpha}_{1,2}(t) - C_{1,02}^* C_{1,01} \frac{\kappa_1}{2} \frac{\omega_{1,10}}{\omega_{r,1}} \tilde{\alpha}_{1,1}(t) \\ & - C_{1,02}^* C_{2,01} \frac{\sqrt{\kappa_1 \gamma_2}}{2} \frac{\omega_{2,10}}{\sqrt{\omega_{r,1} \omega_{a,2}}} e^{ik_{a,1} x_2} \tilde{\alpha}_{2,1}(t - x_2/v_g), \end{aligned} \quad (\text{B6b})$$

$$\begin{aligned} \dot{\tilde{\alpha}}_{2,1}(t) = & -i(\omega_{2,10} - \omega_{a,1})\tilde{\alpha}_{2,1}(t) - iC_{2,01}^* \tilde{f}_{\text{in},2}(t) - |C_{2,01}|^2 \frac{\gamma_2}{4} \frac{\omega_{2,10}}{\omega_{a,2}} \left(\tilde{\alpha}_{2,1}(t) + e^{2ik_{a,1} x_2} \tilde{\alpha}_{2,1}(t - 2x_2/v_g) \right) \\ & - C_{2,01}^* C_{1,01} \frac{\sqrt{\kappa_1 \gamma_2}}{2} \frac{\omega_{1,10}}{\sqrt{\omega_{r,1} \omega_{a,2}}} e^{ik_{a,1} x_2} \tilde{\alpha}_{1,1}(t - x_2/v_g) - C_{2,01}^* C_{1,02} \frac{\sqrt{\kappa_1 \gamma_2}}{2} \frac{\omega_{2,10}}{\sqrt{\omega_{r,1} \omega_{a,2}}} e^{ik_{a,1} x_2} \tilde{\alpha}_{1,2}(t - x_2/v_g), \end{aligned} \quad (\text{B6c})$$

where the appropriate Heaviside theta function factors on the delayed terms are implicit.

We set the initial conditions $\tilde{\alpha}_{1,1}(0) = 1$, $\tilde{\alpha}_{1,2}(0) = \tilde{\alpha}_{2,1}(0) = 0$, $f_\omega(0) = 0$, and use the Euler method for the numerical solution. The Runge-Kutta method applied to the delay differential equations requires accurate interpolations between the time steps [39]. For the Euler method, if the delays x_2/v_g are an integer multiple of the step size, no such interpolation is required. The drawback is a significantly larger number of time steps N_t required to reach convergence. In Fig. 6(b), we use $N_t = 10^{12}$. Compared to the master equation curves in Fig. 6(a), the “steady-state” value in Fig. 6(b) is shifted by about $2 \cdot 10^{-6}$, and the long-time decay rate is positive.

Appendix C: Derivation of the reflection coefficient

In this appendix, we derive the input-output relations corresponding to the master equation (17). The voltage operator in the transmission line is

$$V(x) = -i\sqrt{\frac{\hbar Z_0}{\pi}} \int_0^\infty \sqrt{\omega} (c_\omega - c_\omega^\dagger) \cos(k_\omega x) d\omega, \quad (\text{C1})$$

where Z_0 is the impedance of the transmission line. With the charge number operators $n_m \propto -i(\mathcal{O}_m - \mathcal{O}_m^\dagger)$ for the subsystems attached to the transmission line, the above expression for $V(x)$ determines the interaction Hamiltonian $H_i \propto \sum_{m=1}^N V(x_m) n_m$, resulting in Eq. (2). This can be shown by performing the circuit quantization of the setup.

The voltage operator is split into the right-moving (V_+)

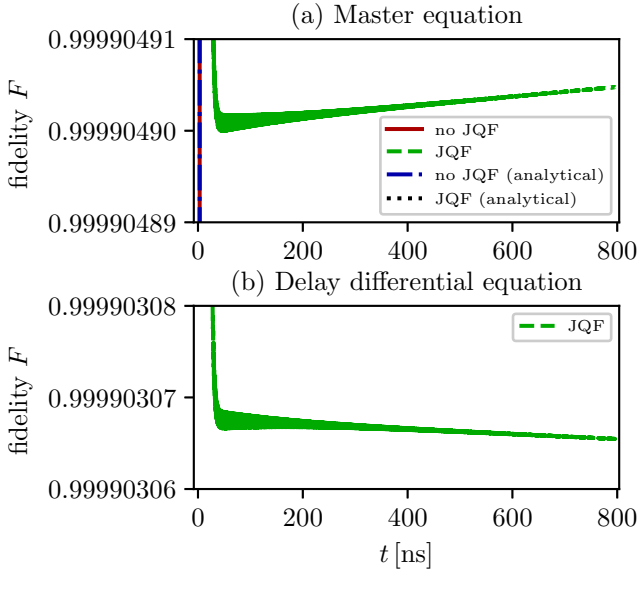


FIG. 6. (a) Zoomed-in version of Fig. 2, using the master equation (17) for the numerical results. Rapid oscillations of the dashed green curve make it appear thick for smaller times. The horizontal dotted black line showing Eq. (24) is about $2 \cdot 10^{-8}$ higher than the upper limit of the vertical axis and hence cannot be seen. (b) The setup with a JQF corresponding to the dashed green curve of (a) calculated using the delay differential equations (B6). In (b), $F = |\tilde{\alpha}_{1,1}(t)|^2$.

and left-moving (V_-) parts, $V(x) = V_+(x) + V_-(x)$, where

$$V_{\pm}(x) = -i\sqrt{\frac{\hbar Z_0}{4\pi}} \int_0^{\infty} \sqrt{\omega} (c_{\omega} e^{\pm ik_{\omega} x} - c_{\omega}^{\dagger} e^{\mp ik_{\omega} x}) d\omega. \quad (C2)$$

We have

$$\begin{aligned} & c_{\omega} e^{\pm ik_{\omega} x} - c_{\omega}^{\dagger} e^{\mp ik_{\omega} x} \\ &= c_{\omega}(0) e^{-i\omega t \pm ik_{\omega} x} - c_{\omega}^{\dagger}(0) e^{i\omega t \mp ik_{\omega} x} - i \sum_{m=1}^N g_m(\omega) \\ & \times \left(\int_0^t \mathcal{O}_m(t-t') \left(e^{-i\omega t' \pm ik_{\omega} x} - e^{i\omega t' \mp ik_{\omega} x} \right) dt' \right. \\ & \left. - \int_0^t \mathcal{O}_m^{\dagger}(t-t') \left(e^{-i\omega t' \pm ik_{\omega} x} - e^{i\omega t' \mp ik_{\omega} x} \right) dt' \right). \end{aligned} \quad (C3)$$

The same comment about Eq. (A3) applies to Eq. (C3)—that additional terms are present due to not making the rotating wave approximation in the Hamiltonian (2).

Only after calculating $c_{\omega} e^{\pm ik_{\omega} x} - c_{\omega}^{\dagger} e^{\mp ik_{\omega} x}$, the resulting expression can be split into two parts involving either creation or annihilation operators. I.e., we write

$$V_{\pm}(x) = \mathcal{V}_{\pm}(x) + \mathcal{V}_{\pm}^{\dagger}(x), \text{ where}$$

$$\begin{aligned} \mathcal{V}_{\pm}(x) &= \mathcal{V}_{\pm,0}(x) \\ & - \sqrt{\frac{\hbar Z_0}{4\pi}} \sum_{m=1}^N \int_0^t \mathcal{O}_m(t-t') \int_0^{\infty} \sqrt{\omega} g_m(\omega) \\ & \times \left(e^{-i\omega t' \pm ik_{\omega} x} - e^{i\omega t' \mp ik_{\omega} x} \right) d\omega dt', \end{aligned} \quad (C4)$$

and

$$\mathcal{V}_{\pm,0}(x) = -i\sqrt{\frac{\hbar Z_0}{4\pi}} \int_0^{\infty} \sqrt{\omega} c_{\omega}(0) e^{-i\omega t \pm ik_{\omega} x} d\omega. \quad (C5)$$

The integral over ω in Eq. (C4) is similar to the integral in Eq. (A5), and we get

$$\begin{aligned} & \int_0^{\infty} \sqrt{\omega} g_m(\omega) \left(e^{-i\omega t' \pm ik_{\omega} x} - e^{i\omega t' \mp ik_{\omega} x} \right) d\omega \\ &= i\pi G_m \left(\dot{\delta} \left(t' \mp \frac{x-x_m}{v_g} \right) + \dot{\delta} \left(t' \mp \frac{x+x_m}{v_g} \right) \right). \end{aligned} \quad (C6)$$

While up to now the calculation for the right-moving and left-moving parts was symmetric, the asymmetry arises after the integration over t' . Using Eq. (A6),

$$\begin{aligned} \mathcal{V}_+(x) &= \mathcal{V}_{+,0}(x) - \sqrt{\frac{\hbar Z_0}{4\pi}} \sum_{m=1}^N (i\pi) G_m \\ & \times \left(\dot{\mathcal{O}}_m \left(t - \frac{x-x_m}{v_g} \right) \theta_H \left(t - \frac{x-x_m}{v_g} \right) \theta_H(x-x_m) \right. \\ & \left. + \dot{\mathcal{O}}_m \left(t - \frac{x+x_m}{v_g} \right) \theta_H \left(t - \frac{x+x_m}{v_g} \right) \right), \end{aligned} \quad (C7a)$$

$$\begin{aligned} \mathcal{V}_-(x) &= \mathcal{V}_{-,0}(x) - \sqrt{\frac{\hbar Z_0}{4\pi}} \sum_{m=1}^N (i\pi) G_m \\ & \times \dot{\mathcal{O}}_m \left(t - \frac{x_m-x}{v_g} \right) \theta_H \left(t - \frac{x_m-x}{v_g} \right) \theta_H(x_m-x). \end{aligned} \quad (C7b)$$

The right-moving part \mathcal{V}_+ has two types of contributions: those that are emitted directly to the right and those that are emitted to the left and then reflected from the boundary at $x = 0$. The left-moving part \mathcal{V}_- only has contributions from the emission directly to the left.

Under the approximations (A10) and (10),

$$\begin{aligned} \mathcal{V}_+(x) &= \mathcal{V}_{+,0}(x) - \sqrt{\frac{\hbar Z_0}{4\pi}} \sum_{m=1}^N \sum_{j,j'} \pi \omega_{m,j'j} G_m C_{m,jj'} \\ & \times \sigma_{m,jj'} \left(\theta_H(x-x_m) e^{ik_{\omega_d}(x-x_m)} + e^{ik_{\omega_d}(x+x_m)} \right), \end{aligned} \quad (C8a)$$

$$\begin{aligned} \mathcal{V}_-(x) &= \mathcal{V}_{-,0}(x) - \sqrt{\frac{\hbar Z_0}{4\pi}} \sum_{m=1}^N \sum_{j,j'} \pi \omega_{m,j'j} G_m C_{m,jj'} \\ & \times \sigma_{m,jj'} \theta_H(x_m-x) e^{ik_{\omega_d}(x_m-x)}. \end{aligned} \quad (C8b)$$

The reflection coefficient is defined to be

$$r = \frac{\text{tr}[\mathcal{V}_+(x_N^+) \rho]}{\text{tr}[\mathcal{V}_-(x_N^+) \rho]}, \quad (\text{C9})$$

where $x_N^+ = x_N + \epsilon$ with $\epsilon > 0$ such that $\epsilon \rightarrow 0$ at the end of the calculation. We assume that the positions x_m are ordered such that they increase with increasing m , and hence x_N^+ is the position just to the right of the last subsystem attached to the transmission line. Hence, $\mathcal{V}_-(x_N^+) = \mathcal{V}_{-,0}(x_N^+)$. Using Eq. (A21), noting that due to Eq. (A24), we have $\text{tr}[\sigma_{m,jj'} \rho] = \text{tr}_s[\sigma_{m,jj'} \tilde{\rho}_s] e^{-i\omega_a t}$, and removing the overall propagation phase $e^{2ik_{\omega_d} x_N^+}$, the reflection coefficient

$$r = 1 - i \sum_{m=1}^N \sum_{j,j'} \frac{\omega_{m,j'j}}{\sqrt{\omega_d \omega_m}} \sqrt{\frac{\Gamma_m}{\hat{n}}} C_{m,jj'} \times \text{tr}_s[\sigma_{m,jj'} \tilde{\rho}_s] \cos(k_{\omega_d} x_m) e^{-i\phi} \quad (\text{C10})$$

is obtained. Writing the photon flux \hat{n} in terms of the reference Rabi frequency Ω_1 using Eq. (12) with $x_1 = 0$, results in the expression (25) of the main text.

Appendix D: Optimal control

In this appendix, we give details about the optimal control used in Sec. V of the main text. The Gaussian-filtered Fourier component function (27) is given by

$$f_p(t) = \sqrt{\frac{2e^{-\omega_p^2 \sigma_f^2/2}}{t_f}} \left(\text{Re} \left[e^{-i\omega_p t} \text{erfi} \left(\frac{\sigma_f^2 \omega_p + it}{\sigma_f \sqrt{2}} \right) \right] - \text{Re} \left[e^{-i\omega_p t} \text{erfi} \left(\frac{\sigma_f^2 \omega_p + i(t - t_f)}{\sigma_f \sqrt{2}} \right) \right] \right), \quad (\text{D1})$$

where $\omega_p = p\pi/t_f$, and erfi is the imaginary error function. For large p , this expression is a difference of two very large numbers and is numerically unstable. Instead, we use the numerical integration to evaluate Eq. (27). The window function in Eq. (26) is given by [28]

$$w(t_n) = G(n) - \frac{G(-0.5)(G(n+L) + G(n-L))}{G(-0.5+L) + G(-0.5-L)}, \quad (\text{D2})$$

where $L = N_t + 1$ is the number of the time points (the interval $[0, t_f]$ is divided into N_t subintervals), and

$$G(n) = \exp \left(- \left(\frac{n - 0.5N_t}{2L\sigma_w} \right)^2 \right). \quad (\text{D3})$$

This expression fulfills $w(0) = w(t_f) = 0$ only approximately, but well enough that the deviation of $\text{Re}[\Omega]$ and

$\text{Im}[\Omega]$ from zero at $t = 0$ and $t = t_f$ is negligible (~ 50 Hz in Fig. 5(b)).

We solve the master equation in the vector form $\dot{\vec{\rho}}_s = L(t)\vec{\rho}_s$ with the 4th order Runge-Kutta method. Defining $\Delta t = t_f/N_t$, $t_n = (\Delta t)n$, $\vec{\rho}_n = \vec{\rho}_s(t_n)$, $L_{1,n} = L(t_n)\Delta t$, $L_{2,n} = L(t_n + (\Delta t)/2)\Delta t$, $L_{3,n} = L(t_{n+1})\Delta t$, it can be written

$$\vec{k}_{1,n} = L_{1,n} \vec{\rho}_n, \quad (\text{D4a})$$

$$\vec{k}_{2,n} = L_{2,n}(\vec{\rho}_n + \vec{k}_{1,n}/2), \quad (\text{D4b})$$

$$\vec{k}_{3,n} = L_{2,n}(\vec{\rho}_n + \vec{k}_{2,n}/2), \quad (\text{D4c})$$

$$\vec{k}_{4,n} = L_{3,n}(\vec{\rho}_n + \vec{k}_{3,n}), \quad (\text{D4d})$$

$$\vec{\rho}_{n+1} = \vec{\rho}_n + \vec{k}_{1,n}/6 + \vec{k}_{2,n}/3 + \vec{k}_{3,n}/3 + \vec{k}_{4,n}/6. \quad (\text{D4e})$$

The reverse mode automatic differentiation applied to this algorithm requires storing or recomputing (during the backward propagation) the vectors $\vec{\rho}_n$, $\vec{k}_{1,n}$, $\vec{k}_{2,n}$, $\vec{k}_{3,n}$, and $\vec{k}_{4,n}$ for all n . The vectors $\vec{\rho}_n$ can be recomputed after the forward propagation by applying the Runge-Kutta method backward in time, starting from $\vec{\rho}_{N_t}$. In our numerical simulations, we store as many of the vectors $\vec{\rho}_n$ as could be fit into memory, uniformly spaced over all the time indices n . The vectors $\vec{\rho}_n$ between the stored ones are recomputed by applying the Runge-Kutta method backward in time. We find that this decreases the numerical error due to inexact recomputation of the vectors $\vec{\rho}_n$.

The vectors $\vec{k}_{1,n}$, $\vec{k}_{2,n}$, $\vec{k}_{3,n}$, and $\vec{k}_{4,n}$ are always recomputed but in an indirect way. We rewrite Eqs. (D4) into the form

$$\vec{\rho}_{n+1} = K_n \vec{\rho}_n, \quad (\text{D5})$$

where

$$K_n = I + \frac{1}{6} L_{1,n} + \frac{1}{3} \left(L_{2,n} + \frac{1}{2} L_{2,n} L_{1,n} \right) + \frac{1}{3} \left(L_{2,n} + \frac{1}{2} L_{2,n} L_{2,n} + \frac{1}{4} L_{2,n} L_{2,n} L_{1,n} \right) + \frac{1}{6} \left(L_{3,n} + L_{3,n} L_{2,n} + \frac{1}{2} L_{3,n} L_{2,n} L_{2,n} + \frac{1}{4} L_{3,n} L_{2,n} L_{2,n} L_{1,n} \right), \quad (\text{D6})$$

and apply the reverse mode automatic differentiation on this form.

The gradient of Eq. (29) at the final time $t = t_f$ is then

$$\frac{\partial \tilde{F}}{\partial a_p} = \tilde{M}_{\tilde{F}}^\dagger \frac{\partial \vec{\rho}_{N_t}}{\partial a_p}, \quad \frac{\partial \tilde{F}}{\partial b_p} = \tilde{M}_{\tilde{F}}^\dagger \frac{\partial \vec{\rho}_{N_t}}{\partial b_p}, \quad (\text{D7})$$

where

$$\frac{\partial \vec{\rho}_n}{\partial a_p} = \frac{\partial K_{n-1}}{\partial a_p} \vec{\rho}_{n-1} + K_{n-1} \frac{\partial \vec{\rho}_{n-1}}{\partial a_p}, \quad (\text{D8a})$$

$$\frac{\partial \vec{\rho}_n}{\partial b_p} = \frac{\partial K_{n-1}}{\partial b_p} \vec{\rho}_{n-1} + K_{n-1} \frac{\partial \vec{\rho}_{n-1}}{\partial b_p}. \quad (\text{D8b})$$

By substituting these equations into themselves for all n and defining the initial value $\vec{\chi}_{N_t}^\dagger = \vec{M}_{\vec{F}}^\dagger$ and the adjoint equation

$$\vec{\chi}_{n-1}^\dagger = \vec{\chi}_n^\dagger K_{n-1}, \quad (\text{D9})$$

we end up with

$$\frac{\partial \tilde{F}}{\partial a_p} = \sum_{n=1}^{N_t} \vec{\chi}_n^\dagger \frac{\partial K_{n-1}}{\partial a_p} \vec{\rho}_{n-1}, \quad (\text{D10a})$$

$$\frac{\partial \tilde{F}}{\partial b_p} = \sum_{n=1}^{N_t} \vec{\chi}_n^\dagger \frac{\partial K_{n-1}}{\partial b_p} \vec{\rho}_{n-1}, \quad (\text{D10b})$$

where the sums are can be efficiently evaluated by starting with $n = N_t$ and propagating $\vec{\chi}_n$ backward using Eq. (D9). We give more details below, but first we summarize the entire procedure:

1. Propagate forward using Eqs. (D4), saving as many of the intermediate values $\vec{\rho}_n$, as can be fit into memory.
2. Initialize $n = N_t$, and use $\vec{\chi}_{N_t}^\dagger = \vec{M}_{\vec{F}}^\dagger$.
3. If $\vec{\rho}_{n-1}$ is not stored in memory, calculate it by propagating Eqs. (D4) backward in time, otherwise use the stored $\vec{\rho}_{n-1}$.
4. Evaluate the scalars given by Eqs. (D14).
5. Add contributions from this n to the gradient using Eqs. (D15) for all a_p and b_p .
6. Calculate $\vec{\chi}_{n-1}$ using Eq. (D17).
7. If $n > 0$, go to step 3 replacing n with $n - 1$. Otherwise, stop.

The above procedure needs a constant number of the computationally expensive matrix-vector multiplications

for every time index n , independent of the number of the parameters a_p and b_p .

To derive the expressions for the above procedure, we first note that

$$(\Delta t) \frac{\partial L(t)}{\partial a_p} = \frac{\partial \text{Re}[\Omega]}{\partial a_p}(t) T_{\text{Re}}, \quad (\text{D11a})$$

$$(\Delta t) \frac{\partial L(t)}{\partial b_p} = \frac{\partial \text{Im}[\Omega]}{\partial b_p}(t) T_{\text{Im}}, \quad (\text{D11b})$$

where, assuming that the density matrix is written as a vector in the row-major form (i.e., $(\tilde{\rho}_s)_{l,l'} = (\vec{\rho}_s)_{lN_b+l'}$, N_b is the Hilbert space basis size, and $0 \leq l, l' \leq N_b - 1$),

$$T_{\text{Re}} = -\frac{i}{\hbar}(\Delta t)(\tilde{H}_{\text{d},\text{Re}} \otimes I - I \otimes \tilde{H}_{\text{d},\text{Re}}^T), \quad (\text{D12a})$$

$$T_{\text{Im}} = -\frac{i}{\hbar}(\Delta t)(\tilde{H}_{\text{d},\text{Im}} \otimes I - I \otimes \tilde{H}_{\text{d},\text{Im}}^T), \quad (\text{D12b})$$

and $\tilde{H}_{\text{d},\text{Re}}$, $\tilde{H}_{\text{d},\text{Im}}$ are given by Eqs. (16). We define the following temporary vectors

$$\vec{l}_{0,n} = T_{\text{Re}} \vec{\rho}_n, \quad \vec{l}_{1,n} = L_{1,n} \vec{\rho}_n, \quad (\text{D13a})$$

$$\vec{l}_{2,n} = L_{2,n} \vec{\rho}_n, \quad \vec{l}_{3,n} = T_{\text{Re}} \vec{l}_{1,n}, \quad (\text{D13b})$$

$$\vec{l}_{4,n} = T_{\text{Re}} \vec{l}_{2,n}, \quad \vec{l}_{5,n} = L_{2,n} \vec{l}_{0,n}, \quad (\text{D13c})$$

$$\vec{l}_{6,n} = L_{2,n} \vec{l}_{1,n}, \quad \vec{l}_{7,n} = L_{2,n} \vec{l}_{3,n}, \quad (\text{D13d})$$

$$\vec{l}_{8,n} = L_{2,n} \vec{l}_{5,n}, \quad \vec{l}_{9,n} = T_{\text{Re}} \vec{l}_{6,n}; \quad (\text{D13e})$$

$$\vec{m}_{0,n} = T_{\text{Im}} \vec{\rho}_n, \quad \vec{m}_{1,n} = L_{1,n} \vec{\rho}_n, \quad (\text{D13f})$$

$$\vec{m}_{2,n} = L_{2,n} \vec{\rho}_n, \quad \vec{m}_{3,n} = T_{\text{Im}} \vec{m}_{1,n}, \quad (\text{D13g})$$

$$\vec{m}_{4,n} = T_{\text{Im}} \vec{m}_{2,n}, \quad \vec{m}_{5,n} = L_{2,n} \vec{m}_{0,n}, \quad (\text{D13h})$$

$$\vec{m}_{6,n} = L_{2,n} \vec{m}_{1,n}, \quad \vec{m}_{7,n} = L_{2,n} \vec{m}_{3,n}, \quad (\text{D13i})$$

$$\vec{m}_{8,n} = L_{2,n} \vec{m}_{5,n}, \quad \vec{m}_{9,n} = T_{\text{Im}} \vec{m}_{6,n}; \quad (\text{D13j})$$

and scalars

$$S_{1,n,\text{Re}} = \vec{\chi}_n^\dagger \left(\frac{1}{6} \vec{l}_{0,n-1} + \frac{1}{6} \vec{l}_{5,n-1} + \frac{1}{12} \vec{l}_{8,n-1} + \frac{1}{24} L_{3,n-1} \vec{l}_{8,n-1} \right), \quad (\text{D14a})$$

$$S_{2,n,\text{Re}} = \vec{\chi}_n^\dagger \left(\frac{2}{3} \vec{l}_{0,n-1} + \frac{1}{6} \vec{l}_{3,n-1} + \frac{1}{6} \vec{l}_{4,n-1} + \frac{1}{6} \vec{l}_{5,n-1} + \frac{1}{12} \vec{l}_{9,n-1} + \frac{1}{12} \vec{l}_{7,n-1} \right. \quad (\text{D14b})$$

$$\left. + \frac{1}{6} L_{3,n-1} \left(\vec{l}_{0,n-1} + \frac{1}{2} \vec{l}_{4,n-1} + \frac{1}{2} \vec{l}_{5,n-1} + \frac{1}{4} \vec{l}_{9,n-1} + \frac{1}{4} \vec{l}_{7,n-1} \right) \right),$$

$$S_{3,n,\text{Re}} = \vec{\chi}_n^\dagger \left(\frac{1}{6} \vec{l}_{0,n-1} + \frac{1}{6} \vec{l}_{4,n-1} + \frac{1}{12} T_{\text{Re}} L_{2,n-1} \left(\vec{l}_{2,n-1} + \frac{1}{2} \vec{l}_{6,n-1} \right) \right), \quad (\text{D14c})$$

$$S_{1,n,\text{Im}} = \vec{\chi}_n^\dagger \left(\frac{1}{6} \vec{m}_{0,n-1} + \frac{1}{6} \vec{m}_{5,n-1} + \frac{1}{12} \vec{m}_{8,n-1} + \frac{1}{24} L_{3,n-1} \vec{m}_{8,n-1} \right), \quad (\text{D14d})$$

$$S_{2,n,\text{Im}} = \vec{\chi}_n^\dagger \left(\frac{2}{3} \vec{m}_{0,n-1} + \frac{1}{6} \vec{m}_{3,n-1} + \frac{1}{6} \vec{m}_{4,n-1} + \frac{1}{6} \vec{m}_{5,n-1} + \frac{1}{12} \vec{m}_{9,n-1} + \frac{1}{12} \vec{m}_{7,n-1} + \frac{1}{6} L_{3,n-1} \left(\vec{m}_{0,n-1} + \frac{1}{2} \vec{m}_{4,n-1} + \frac{1}{2} \vec{m}_{5,n-1} + \frac{1}{4} \vec{m}_{9,n-1} + \frac{1}{4} \vec{m}_{7,n-1} \right) \right), \quad (\text{D14e})$$

$$S_{3,n,\text{Im}} = \vec{\chi}_n^\dagger \left(\frac{1}{6} \vec{m}_{0,n-1} + \frac{1}{6} \vec{m}_{4,n-1} + \frac{1}{12} T_{\text{Re}} L_{2,n-1} \left(\vec{m}_{2,n-1} + \frac{1}{2} \vec{m}_{6,n-1} \right) \right). \quad (\text{D14f})$$

The above definitions allow us to write

$$\begin{aligned} \vec{\chi}_n^\dagger \frac{\partial K_{n-1}}{\partial a_p} \vec{\rho}_{n-1} &= \frac{\partial \text{Re}[\Omega]}{\partial a_p} (t_{n-1}) S_{1,n,\text{Re}} \\ &+ \frac{\partial \text{Re}[\Omega]}{\partial a_p} (t_{n-1} + (\Delta t)/2) S_{2,n,\text{Re}} \\ &+ \frac{\partial \text{Re}[\Omega]}{\partial a_p} (t_n) S_{3,n,\text{Re}}, \end{aligned} \quad (\text{D15a})$$

$$\begin{aligned} \vec{\chi}_n^\dagger \frac{\partial K_{n-1}}{\partial b_p} \vec{\rho}_{n-1} &= \frac{\partial \text{Im}[\Omega]}{\partial b_p} (t_{n-1}) S_{1,n,\text{Im}} \\ &+ \frac{\partial \text{Im}[\Omega]}{\partial b_p} (t_{n-1} + (\Delta t)/2) S_{2,n,\text{Im}} \\ &+ \frac{\partial \text{Im}[\Omega]}{\partial b_p} (t_n) S_{3,n,\text{Im}}. \end{aligned} \quad (\text{D15b})$$

The backward propagation in Eq. (D9) can also be written explicitly. Define

$$\vec{\mu}_{1,n} = L_{2,n-1}^\dagger \vec{\chi}_n, \quad \vec{\mu}_{2,n} = L_{3,n-1}^\dagger \vec{\chi}_n, \quad (\text{D16a})$$

$$\vec{\mu}_{3,n} = L_{2,n-1}^\dagger \vec{\mu}_{1,n}, \quad \vec{\mu}_{4,n} = L_{2,n-1}^\dagger \vec{\mu}_{2,n}, \quad (\text{D16b})$$

$$\vec{\mu}_{5,n} = L_{2,n-1}^\dagger \vec{\mu}_{4,n}. \quad (\text{D16c})$$

Then

$$\begin{aligned} \vec{\chi}_{n-1} &= \vec{\chi}_n \\ &+ L_{1,n-1}^\dagger \left(\frac{1}{6} \vec{\chi}_n + \frac{1}{6} \vec{\mu}_{1,n} + \frac{1}{12} \vec{\mu}_{3,n} + \frac{1}{24} \vec{\mu}_{5,n} \right) \\ &+ \frac{2}{3} \vec{\mu}_{1,n} + \frac{1}{6} \vec{\mu}_{2,n} + \frac{1}{6} \vec{\mu}_{3,n} + \frac{1}{6} \vec{\mu}_{4,n} + \frac{1}{12} \vec{\mu}_{5,n}. \end{aligned} \quad (\text{D17})$$

[1] F. Arute, K. Arya, R. Babbush, D. Bacon, J. C. Bardin, R. Barends, R. Biswas, S. Boixo, F. G. S. L. Brandao, D. A. Buell, B. Burkett, Y. Chen, Z. Chen, B. Chiaro, R. Collins, W. Courtney, A. Dunsworth, E. Farhi, B. Foxen, A. Fowler, C. Gidney, M. Giustina, R. Graff, K. Guerin, S. Habegger, M. P. Harrigan, M. J. Hartmann, A. Ho, M. Hoffmann, T. Huang, T. S. Humble, S. V. Isakov, E. Jeffrey, Z. Jiang, D. Kafri, K. Kechedzhi, J. Kelly, P. V. Klimov, S. Knysh, A. Korotkov, F. Kostritsa, D. Landhuis, M. Lindmark, E. Lucero, D. Lyakh, S. Mandrà, J. R. McClean, M. McEwen, A. Megrant, X. Mi, K. Michelsen, M. Mohseni, J. Mutus, O. Naaman, M. Neeley, C. Neill, M. Y. Niu, E. Ostby, A. Petukhov, J. C. Platt, C. Quintana, E. G. Rieffel, P. Roushan, N. C. Rubin, D. Sank, K. J. Satzinger, V. Smelyanskiy, K. J. Sung, M. D. Trevithick, A. Vainsencher, B. Villalonga, T. White, Z. J. Yao, P. Yeh, A. Zalcman, H. Neven, and J. M. Martinis, *Quantum supremacy using a programmable superconducting processor*, *Nature* **574**, 505 (2019).

[2] E. J. Zhang, S. Srinivasan, N. Sundaresan, D. F. Bogorin, Y. Martin, J. B. Hertzberg, J. Timmerwilke, E. J. Pritchett, J.-B. Yau, C. Wang, W. Landers, E. P. Lewandowski, A. Narasgond, S. Rosenblatt, G. A. Keefe, I. Lauer, M. B. Rothwell, D. T. McClure, O. E. Dial, J. S. Orcutt, M. Brink, and J. M. Chow, *High-fidelity superconducting quantum processors via laser-annealing of transmon qubits* (2020), arXiv:2012.08475 [quant-ph].

[3] P. Jurcevic, A. Javadi-Abhari, L. S. Bishop, I. Lauer, D. F. Bogorin, M. Brink, L. Capelluto, O. Günlük, T. Itoko, N. Kanazawa, A. Kandala, G. A. Keefe, K. Krsulich, W. Landers, E. P. Lewandowski, D. T. McClure, G. Nannicini, A. Narasgond, H. M. Nayfeh, E. Pritchett, M. B. Rothwell, S. Srinivasan, N. Sundaresan, C. Wang, K. X. Wei, C. J. Wood, J.-B. Yau, E. J. Zhang, O. E. Dial, J. M. Chow, and J. M. Gambetta, *Demonstration of quantum volume 64 on a superconducting quantum computing system*, *Quantum Science and Technology* **6**, 025020 (2021).

[4] M. Gong, S. Wang, C. Zha, M.-C. Chen, H.-L. Huang, Y. Wu, Q. Zhu, Y. Zhao, S. Li, S. Guo, H. Qian, Y. Ye, F. Chen, C. Ying, J. Yu, D. Fan, D. Wu, H. Su, H. Deng, H. Rong, K. Zhang, S. Cao, J. Lin, Y. Xu, L. Sun, C. Guo, N. Li, F. Liang, V. M. Bastidas, K. Nemoto, W. J. Munro, Y.-H. Huo, C.-Y. Lu, C.-Z. Peng, X. Zhu, and J.-W. Pan, *Quantum walks on a programmable two-dimensional 62-qubit superconducting processor*, *Science* **372**, 948 (2021).

[5] Q. Zhu, S. Cao, F. Chen, M.-C. Chen, X. Chen, T.-H. Chung, H. Deng, Y. Du, D. Fan, M. Gong, C. Guo, C. Guo, S. Guo, L. Han, L. Hong, H.-L. Huang, Y.-H. Huo, L. Li, N. Li, S. Li, Y. Li, F. Liang, C. Lin, J. Lin, H. Qian, D. Qiao, H. Rong, H. Su, L. Sun, L. Wang, S. Wang, D. Wu, Y. Wu, Y. Xu, K. Yan, W. Yang, Y. Yang, Y. Ye, J. Yin, C. Ying, J. Yu, C. Zha, C. Zhang, H. Zhang, K. Zhang, Y. Zhang, H. Zhao, Y. Zhao, L. Zhou, C.-Y. Lu, C.-Z. Peng, X. Zhu, and J.-W. Pan, *Quantum computational advantage via 60-qubit 24-cycle random circuit sampling*, *Science Bulletin* **67**, 240 (2022).

[6] M. D. Reed, B. R. Johnson, A. A. Houck, L. DiCarlo, J. M. Chow, D. I. Schuster, L. Frunzio, and R. J. Schoelkopf, *Fast reset and suppressing spontaneous emission of a superconducting qubit*, *Applied Physics Letters* **96**, 203110 (2010).

[7] E. Jeffrey, D. Sank, J. Y. Mutus, T. C. White, J. Kelly, R. Barends, Y. Chen, Z. Chen, B. Chiaro, A. Dunsworth, A. Megrant, P. J. J. O’Malley, C. Neill, P. Roushan, A. Vainsencher, J. Wenner, A. N. Cleland, and J. M. Martinis, *Fast Accurate State Measurement with Superconducting Qubits*, *Phys. Rev. Lett.* **112**, 190504 (2014).

[8] N. T. Bronn, Y. Liu, J. B. Hertzberg, A. D. Córcoles, A. A. Houck, J. M. Gambetta, and J. M. Chow, *Broadband filters for abatement of spontaneous emission in circuit quantum electrodynamics*, *Applied Physics Letters* **107**, 172601 (2015).

[9] Y. Sunada, S. Kono, J. Ilves, S. Tamate, T. Sugiyama, Y. Tabuchi, and Y. Nakamura, *Fast readout and reset of a superconducting qubit coupled to a resonator with an intrinsic Purcell filter* (2022), arXiv:2202.06202 [quant-ph].

[10] K. Koshino, S. Kono, and Y. Nakamura, *Protection of a Qubit via Subradiance: A Josephson Quantum Filter*, *Phys. Rev. Applied* **13**, 014051 (2020).

[11] S. Kono, K. Koshino, D. Lachance-Quirion, A. F. van Loo, Y. Tabuchi, A. Noguchi, and Y. Nakamura, *Breaking the trade-off between fast control and long lifetime of a superconducting qubit*, *Nature Communications* **11**, 3683 (2020).

[12] R. Barends, J. Kelly, A. Megrant, A. Veitia, D. Sank, E. Jeffrey, T. C. White, J. Mutus, A. G. Fowler, B. Campbell, Y. Chen, Z. Chen, B. Chiaro, A. Dunsworth, C. Neill, P. O’Malley, P. Roushan, A. Vainsencher, J. Wenner, A. N. Korotkov, A. N. Cleland, and J. M. Martinis, *Superconducting quantum circuits at the surface code threshold for fault tolerance*, *Nature* **508**, 500 (2014).

[13] M. Jerger, S. Poletto, P. Macha, U. Hübner, E. Il’ichev, and A. V. Ustinov, *Frequency division multiplexing readout and simultaneous manipulation of an array of flux qubits*, *Applied Physics Letters* **101**, 042604 (2012).

[14] Y. Chen, D. Sank, P. O’Malley, T. White, R. Barends, B. Chiaro, J. Kelly, E. Lucero, M. Mariantoni, A. Megrant, C. Neill, A. Vainsencher, J. Wenner, Y. Yin, A. N. Cleland, and J. M. Martinis, *Multiplexed dispersive readout of superconducting phase qubits*, *Applied Physics Letters* **101**, 182601 (2012).

[15] D. Rosenberg, D. Kim, R. Das, D. Yost, S. Gustavsson, D. Hover, P. Krantz, A. Melville, L. Racz, G. O. Samach, S. J. Weber, F. Yan, J. L. Yoder, A. J. Kerman, and W. D. Oliver, *3D integrated superconducting qubits*, *npj Quantum Information* **3**, 42 (2017).

[16] D. Lachance-Quirion, S. P. Wolski, Y. Tabuchi, S. Kono, K. Usami, and Y. Nakamura, *Entanglement-based single-shot detection of a single magnon with a superconducting qubit*, *Science* **367**, 425 (2020).

[17] J. R. Ott, M. Wubs, P. Lodahl, N. A. Mortensen, and R. Kaiser, *Cooperative fluorescence from a strongly driven dilute cloud of atoms*, *Phys. Rev. A* **87**, 061801(R) (2013).

[18] R. H. Lehmberg, *Radiation from an N-Atom System. I. General Formalism*, *Phys. Rev. A* **2**, 883 (1970).

[19] K. Wódkiewicz and J. Eberly, *Markovian and non-Markovian behavior in two-level atom fluorescence*, *Annals of Physics* **101**, 574 (1976).

[20] I. de Vega and D. Alonso, *Dynamics of non-Markovian open quantum systems*, *Rev. Mod. Phys.* **89**, 015001 (2017).

[21] J. M. Gambetta, in *Quantum Information Processing Lecture Notes*, 44th IFF Spring school 2013 (2013).

[22] J. Gambetta, W. A. Braff, A. Wallraff, S. M. Girvin, and R. J. Schoelkopf, *Protocols for optimal readout of qubits using a continuous quantum nondemolition measurement*, *Phys. Rev. A* **76**, 012325 (2007).

[23] H. M. Wiseman and G. J. Milburn, *Quantum Measurement and Control* (Cambridge University Press, 2009).

[24] S. Masuda and K. Koshino, *Effects of higher levels of qubits on control of qubit protected by a Josephson quantum filter*, *New Journal of Physics* **23**, 013006 (2021).

[25] P. Doria, T. Calarco, and S. Montangero, *Optimal control technique for many-body quantum dynamics*, *Phys. Rev. Lett.* **106**, 190501 (2011).

[26] F. Motzoi, J. M. Gambetta, S. T. Merkel, and F. K. Wilhelm, *Optimal control methods for rapidly time-varying Hamiltonians*, *Phys. Rev. A* **84**, 022307 (2011).

[27] S. Machnes, E. Assémat, D. Tannor, and F. K. Wilhelm, *Tunable, flexible, and efficient optimization of control pulses for practical qubits*, *Phys. Rev. Lett.* **120**, 150401 (2018).

[28] S. Starosielec and D. Hägele, *Discrete-time windows with minimal RMS bandwidth for given RMS temporal width*, *Signal Processing* **102**, 240 (2014).

[29] H. Takahasi and M. Mori, *Double Exponential Formulas for Numerical Integration*, *Publ. Res. Inst. Math. Sci.* **9**, 721 (1973).

[30] Y. Evtushenko, *Computation of exact gradients in distributed dynamic systems*, *Optimization Methods and Software* **9**, 45 (1998).

[31] A. Walther, *Automatic Differentiation of Explicit Runge-Kutta Methods for Optimal Control*, *Comput. Optim. Appl.* **36**, 83–108 (2007).

[32] R. Kosloff, S. Rice, P. Gaspard, S. Tersigni, and D. Tannor, *Wavepacket dancing: Achieving chemical selectivity by shaping light pulses*, *Chemical Physics* **139**, 201 (1989).

[33] J. Somlói, V. A. Kazakov, and D. J. Tannor, *Controlled dissociation of I_2 via optical transitions between the X and B electronic states*, *Chemical Physics* **172**, 85 (1993).

[34] J. Nocedal, *Updating Quasi-Newton Matrices with Limited Storage*, *Mathematics of Computation* **35**, 773 (1980).

[35] S. G. Johnson, *The NLopt nonlinear-optimization package*.

[36] W. D. Kalfus, D. F. Lee, G. J. Ribeill, S. D. Fallek, A. Wagner, B. Donovan, D. Ristè, and T. A. Ohki, *High-fidelity control of superconducting qubits using direct microwave synthesis in higher nyquist zones*, *IEEE Transactions on Quantum Engineering* **1**, 1 (2020).

[37] L. Stefanazzi, K. Treptow, N. Wilcer, C. Stoughton, S. Montella, C. Bradford, G. Cancelo, S. Saxena, H. Arnaldi, S. Sussman, A. Houck, A. Agrawal, H. Zhang, C. Ding, and D. I. Schuster, *The QICK (Quantum Instrumentation Control Kit): Readout and control for qubits and detectors* (2021), arXiv:2110.00557 [quant-ph].

[38] K. J. Blow, R. Loudon, S. J. D. Phoenix, and T. J. Shepherd, *Continuum fields in quantum optics*, *Phys. Rev. A* **42**, 4102 (1990).

[39] H. J. Oberle and H. J. Pesch, *Numerical treatment*

of delay differential equations by Hermite Interpolation,
Numerische Mathematik **37**, 235 (1981).